



Radiology of Kidney Transplantation

Christopher G. Roth, Daniel J. Mizrahi, and
Laurence Needleman

Contents

Introduction	250
Renal Donor Imaging	252
Renal Recipient Imaging	262
Ultrasound	264
CT	272
MRI	276
Renal Scintigraphy	279
Interventional Radiology	283
Conclusion	285
Cross-References	287
References	287

Abstract

Radiologic imaging procedures include a wide array of modalities and many are indicated in the diagnosis and treatment of renal transplant recipients and donors. In the renal donor candidate, CT is the optimal imaging modality for anatomic assessment and MRI is a potential alternative. CT is also utilized for the vascular evaluation of recipients at risk for peripheral vascular disease. Imaging modalities are

central to the diagnosis and treatment of renal transplantation complications. Ultrasound (US) is the first-line imaging modality to evaluate allograft dysfunction with utility for identifying parenchymal and vascular complications, fluid collections, and urinary complications. While renal scintigraphy provides an alternative to US in assessing graft dysfunction and detecting these complications, CT and MRI serve an ancillary role. Interventional radiology procedures in the posttransplant setting include a variety of diagnostic and therapeutic procedures. Arteriography confirms arterial disease and precedes angioplasty/stenting for renal artery stenosis and

C. G. Roth (✉) · D. J. Mizrahi · L. Needleman
Sidney Kimmel Medical College, Thomas Jefferson
University, Philadelphia, PA, USA
e-mail: christopher.roth@jefferson.edu;
daniel.mizrahi@jefferson.edu; larryneedleman@me.com

embolization for arteriovenous fistula and pseudoaneurysm. Urologic complications are treated with procedures such as percutaneous nephrostomy, urinary stent placement, or stricture angioplasty. Image-guided fluid collection drainage is usually accomplished with ultrasound, reserving CT for cases in which a poor acoustic window limits US.

Keywords

Radiology · Ultrasound · Computed tomography · Magnetic resonance imaging · Nuclear scintigraphy · PET/CT · Interventional radiology · Renal transplantation

Introduction

Imaging figures prominently throughout the renal transplantation life cycle from donor and recipient workup to posttransplant surveillance and management. The noninvasive nature of most diagnostic procedures and minimally invasive nature of interventional procedures make radiologic techniques central to patient care.

Imaging utilization incurs cost and potential complications, depending on the modality, which do factor into the management approach (Fig. 1). X-ray plays an ancillary role in renal transplantation imaging – as a quick survey to identify or

exclude gross complications. Computed tomography (CT) and ultrasound (US) constitute the core diagnostic imaging modalities in managing renal transplantation. CT employs an X-ray tube rotating within a gantry as a means to obtain a volume of image data reconstructed into axial images by convention, but easily reformatted into sagittal, coronal, or any oblique plane desired. Unenhanced CT images portray anatomy clearly, but lack contrast between visceral organs and other soft tissue densities. Tissue contrast is magnified with the administration of intravenous iodinated contrast material because normal and abnormal tissues exhibit different enhancement patterns (Fig. 2). Oral contrast, in the form of either barium or iodine suspension, is administered to isolate bowel from surrounding normal structures and fluid collections, abscesses, etc. The low risk, convenience, and speed of CT tend to preempt consideration of the potential downsides – ionizing radiation, cost and potential nephrotoxicity, and allergic reactions related to iodinated contrast media. However, nephrotoxicity risk only mounts with advanced renal dysfunction and only relevant with an estimated glomerular filtration rate (eGFR) of less than 30–45 mL/min/1.73 m² (Davenport et al. 2013).

US has no adverse side effects at a lower cost. Additionally, the native and transplant kidneys – in addition to other visceral organs – are well-imaged sonographically. The major caveat is the operator-

Modality	Cost	Radiation	Nephrotoxicity	Other Side Effects	Imaging Medium
X-Ray	+	+	None	None	Ionizing radiation
Ultrasound	++	-	None	None	Sound waves
CT	+++	+++	+ (eGFR >= 40-45 poses minimal risk)	Contrast allergy	Ionizing radiation
MRI	++++	-	None	Interaction with implanted devices and ferromagnetic objects; NSF in ESRD; contrast allergy	Radiofrequency waves in a strong magnetic field
NM	+++	+++	None	None	Gamma rays
IR	+++++	+++	+	Bleeding, organ injury, infection (depending on the procedure); contrast allergy	Ionizing radiation and/or sound waves

Fig. 1 Imaging modalities in renal transplantation

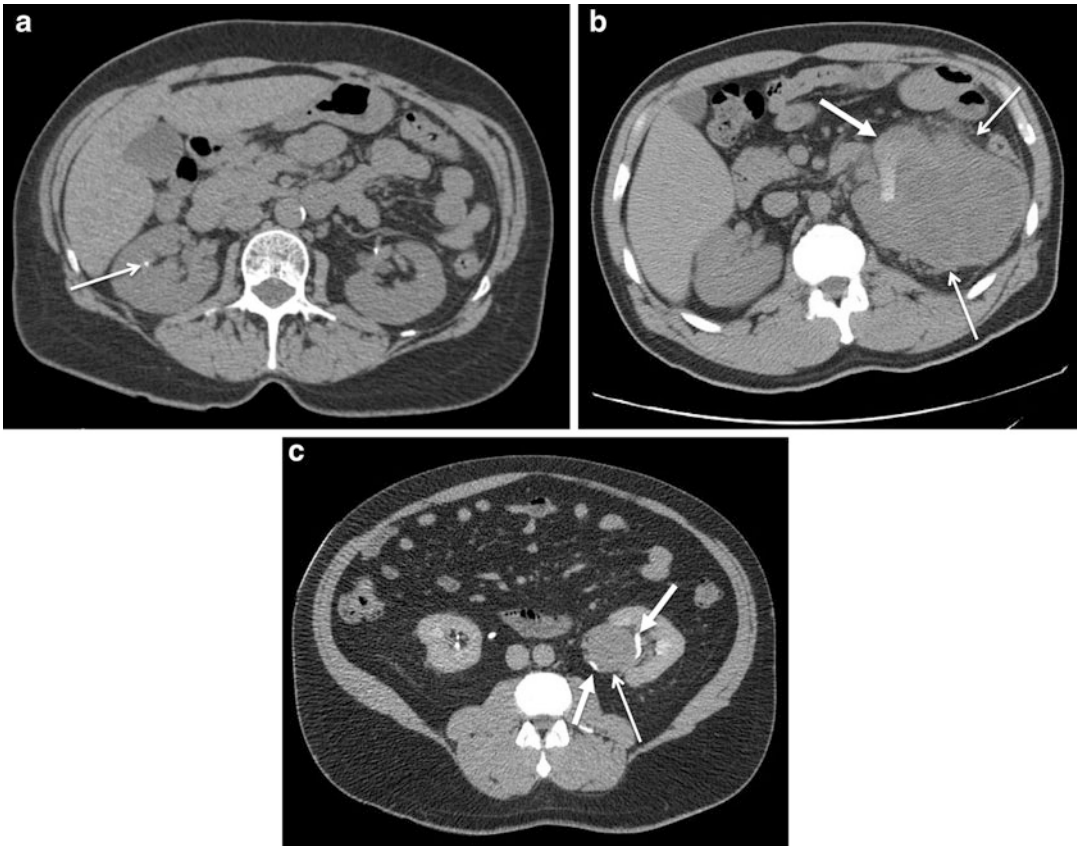


Fig. 2 Examples of CT images. (a) An axial image from a CT of the abdomen and pelvis without either oral or intravenous contrast shows a punctate, nonobstructing right renal calculus (*arrow*). (b) Another unenhanced CT image in a different patient with a chromophobe-type RCC demonstrates a large, heterogeneous mass (*arrows*) replacing the left kidney; hyperdense material in the left

renal collecting system (*thick arrow*) represents excreted gadolinium from a preceding MRI. (c) The axial post-contrast pyelographic phase image in another patient with a chromophobe-type RCC shows a small, exophytic mass (*arrow*) extending into the renal hilum displacing the renal collecting system (*thick arrows*)

dependency of US; obtaining diagnostic US images requires mastery of the modality and of the relevant anatomy. Also, generating diagnostic US studies is fairly time-consuming (exam duration ranges from 15 or 20 min to 45 min, depending on the type of study) and requires careful attention to technique. US technical considerations include optimal position and machine settings, understanding when and how to use Doppler US including how to sample vessels and measure various parameters correctly (e.g., velocity, resistive index, acceleration, etc.). Nonetheless, US is the first-line imaging modality for most indications.

While ultrasound is the first-line modality to evaluate renal allograft failure, renal scintigraphy

is a potentially useful alternative posing no threat to the allograft. Renal scintigraphy involves the intravenous administration of a radioisotope, which emits gamma rays detected with a gamma camera, yielding images that illustrate the distribution of the radioactive agent. Serial images are obtained over the course of approximately 30 min and used to assess arterial perfusion, followed by parenchymal uptake and excretion.

Magnetic resonance imaging (MRI) plays an ancillary role in the setting of renal transplant imaging, although it offers advantages by avoiding ionizing radiation and nephrotoxicity. Its relatively high cost and the availability and diagnostic accuracy of other modalities generally relegate MRI to the role

of problem-solving. While gadolinium contrast agents pose no risk of nephrotoxicity, in the setting of end-stage renal disease (ESRD) and acute renal injury, gadolinium contrast agents potentially risk nephrogenic systemic fibrosis (NSF). However, the greater stability of modern gadolinium agents mitigates this risk. Virtually all reported cases of NSF were associated with older contrast agents (Thomsen et al. 2013; Morcos 2014; Yang et al. 2012). Notwithstanding, ESRD with eGFR below 30 constitutes a relative contraindication to gadolinium administration. Most NSF cases have occurred with eGFR levels below 15 (ACR 2013).

Interventional radiology (IR) provides a wide array of procedures for diagnostic and therapeutic management of renal transplantation (Fig. 3). These procedures are generally performed with image guidance – either ultrasound, CT, or fluoroscopy (and many modern IR suites also feature rotational angiography, or cone beam CT, which generates 3D CT-like images). Diagnostic IR procedures include renal biopsy, percutaneous nephrostography (to identify the site of a urinary leak), percutaneous catheter-directed angiography to identify and characterize vascular complications, and percutaneous fluid collection aspiration. Many of these procedures offer concurrent treatment strategies: drainage of fluid collections, diversion of flow in urinary leaks, transcatheter embolization of vascular injuries, and angioplasty of renal artery stenosis (RAS).

Renal Donor Imaging

While renal transplant recipients have many imaging needs, imaging plays a crucial role in the preoperative management of the renal transplant donor. Anatomic characterization is the chief imaging objective in the donor to determine the kidney more safely transplanted. Vascular anatomic considerations figure prominently in the surgical approach and the Organ Procurement and Transplantation Network (OPTN) sanctions the use of CT, MRI, or angiography for the anatomic donor workup (OPTN 2016). Both CT and MRI accurately depict arterial and venous anatomy. The occasional missed small accessory renal artery is less common with newer technology (Rankin et al. 2001; Kawamoto et al. 2003). The superior spatial resolution of CT explains its wider acceptance for preoperative renal donor assessment (Singh and Sahani 2008). The CT protocol involves several series before and after intravenous contrast administration in order to assess the parenchyma, vascular structures, collecting systems and ureters, and other relevant factors (i.e., stones and extraurinary findings). Noncontrast scan of the abdomen and pelvis is followed by an acquisition obtained during arterial enhancement and a third minutes later during the excretory phase. The pre-contrast phase image set detects renal calculi and serves as a reference standard to determine the degree of enhancement of renal tissue and unexpected lesions. The arterial-phase image set

Procedure	Objective
Arteriography	Renal/iliac artery stenosis: diagnosis and treatment (angioplasty and stenting)
	Pseudoaneurysm and AVF: diagnosis and treatment (superselective embolization)
Percutaneous nephrostomy	Urinary obstruction: diagnosis, drainage and treatment (angioplasty)
	Urinary leak: diagnosis, urinary diversion and treatment (nephroureteral stent)
Image-guided percutaneous biopsy (usually US)	Diagnosis of graft failure
Image-guided drainage of fluid collections	Diagnosis and treatment

Fig. 3 Interventional radiologic procedures in renal transplantation

demonstrates arterial anatomy and renal tissue enhancement and the delayed-phase image set highlights the renal collecting system, ureters, and bladder. Venous anatomy is depicted on all images sets (some favor adding an acquisition between the arterial- and delayed-phases at the cost of adding ionizing radiation exposure). Vascular and urographic anatomy is optimally displayed with the benefit of image postprocessing in the forms of 3D volume-rendered angiographic, maximal intensity projectional (MIP), and curved planar reformatted images (Fig. 4).

CT imaging provides information regarding various potential donor contraindications and considerations regarding the surgical approach (Fig. 5). Parenchymal features excluding donation include: unilateral agenesis, horseshoe kidney

(Fig. 6), cortical atrophy, polycystic disease, medullary sponge kidney, and papillary necrosis (Sebastià et al. 2010). Other features inform pre-surgical planning, such as relative kidney size (discussed further in the volumetry section), renal ectopia, and ureteropelvic junction (UPJ) stenosis. Renal arterial anatomy and anatomic variations influence the surgical approach and require image postprocessing software to characterize and illustrate to guide surgery. While 71% of kidneys have single renal artery supply, 24% have dual supply, and the remaining 5% with more than two renal arteries are not suitable for transplantation, except when one of three arteries is a small superior polar artery less than 2 mm in diameter (because only a small segment of tissue is sacrificed). Lower polar vessels often supply the

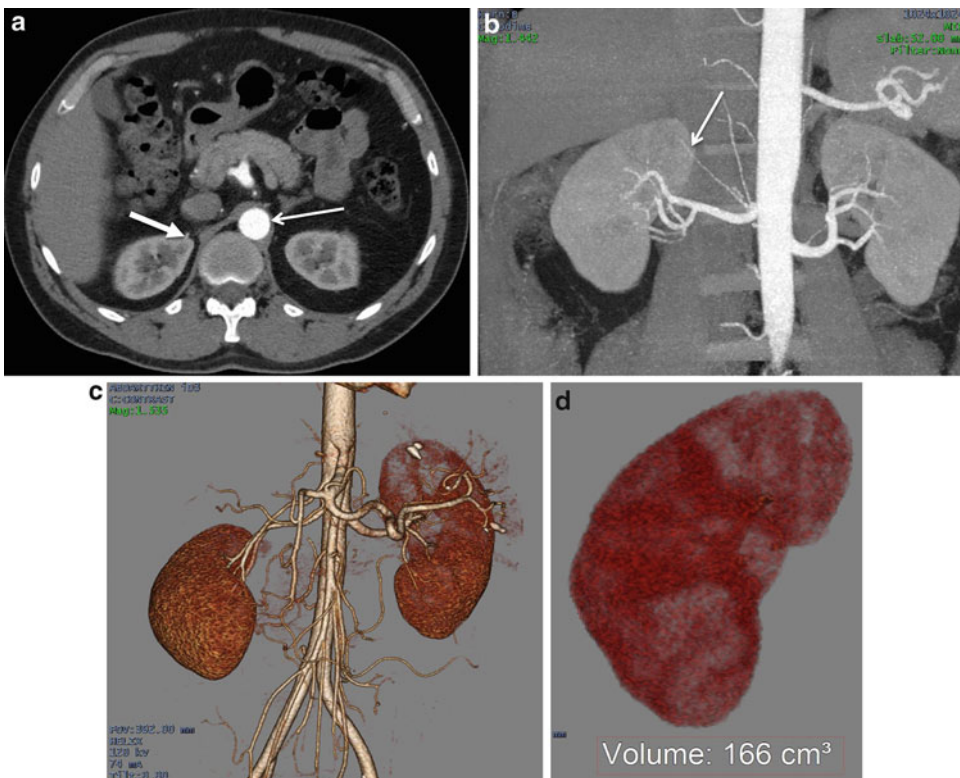


Fig. 4 CT images in preoperative renal donor transplantation. (a) The axial image from a CTA in a renal transplant donor candidate shows avid aortic enhancement (*arrow*) and a small transcortical penetrating arterial branch to the right renal upper pole (*thick arrow*). (b) The corresponding maximal intensity image demonstrates the course of the

small right upper polar branch to better advantage (*arrow*). (c) A 3D volume-rendered postprocessed image in a different patient provides an overview of the arterial and renal anatomy. (d) From the CTA image dataset, using dedicated software, the kidneys are extracted and renal volumes are calculated

Absolute Contraindications	Surgical Considerations
Significant unilateral atrophy	Renal location and size
Horseshoe kidney	Number of renal arteries and veins
Solitary kidney	Types of accessory arteries
Polycystic disease	First arterial segmentary bifurcation
Significant atherosclerotic disease	Renal venous anatomy/anomalies
Fibromuscular dysplasia	Presence of arterial disease
Renal tumors	Number/location/size of renal cysts and angiomyolipomas
Extensive nephrolithiasis	Number/location/size of renal calculi
Active infection	Number/location/size/stage of renal tumors
More than 2 or 3 renal arteries	Upper urinary tract evaluation

Fig. 5 Imaging objectives in the renal transplant donor workup

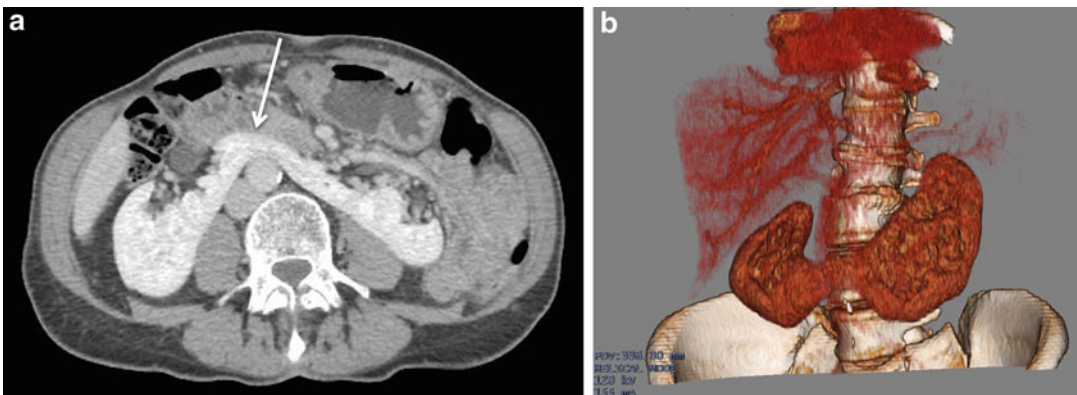


Fig. 6 Horseshoe kidney. **(a)** Axial postcontrast CT image shows a horseshoe kidney with enhancing renal tissue (*arrow*) interconnecting the two moieties anterior to the

aorta and IVC. **(b)** 3D volume-rendered postprocessed image provides an anatomic overview of the horseshoe kidney and surrounding anatomy

upper urinary tract (Uflacker 2006). With multiple renal arteries, the largest caliber is the main renal artery and the other(s) is/are accessory arteries (Türkvatan et al. 2009). With dual arterial supply, the ostial-bifurcation segment length of each vessel factors into the decision to favor end-to-end or side-to-side anastomosis over double arterial anastomosis to the recipient iliac artery. Arteries less than 3 mm in diameter are technically challenging and experience worse outcomes post-anastomosis with a higher incidence of thrombosis. Segmentary bifurcation anatomy has surgical implications and three measurements on CT images help to inform the surgical approach:

1. Right renal artery origin to first segmentary bifurcation
2. Right lateral inferior vena cava (IVC) margin to first segmentary bifurcation
3. Left renal artery origin to first segmentary bifurcation

Retrocaval right segmentary anatomy – with a prevalence of 10–12% (Kawamoto et al. 2004) – complicates the surgical approach because of the threat of vascular injury. For this reason, early, retrocaval right renal artery bifurcation is tantamount to dual artery supply, from a surgical standpoint; the same is true of the left renal artery

with bifurcation within 1–1.5 cm of the origin (Fig. 7).

Another renal artery anatomical characteristic to consider is the entry point, either: (1) hilar (most common), (2) polar, or (3) capsular, surrounding the kidney (Fig. 8). Small upper polar arteries below the size threshold (2 mm) for

successful anastomosis are safely sacrificed because of the small volume of infarcted tissue – less than 10% (Satyapal et al. 2001). However, sacrificing lower polar arteries is contraindicated by the fact that they often provide supply to the upper collecting system, threatening pyeloureteral necrosis when ligated or thrombosed. Capsular

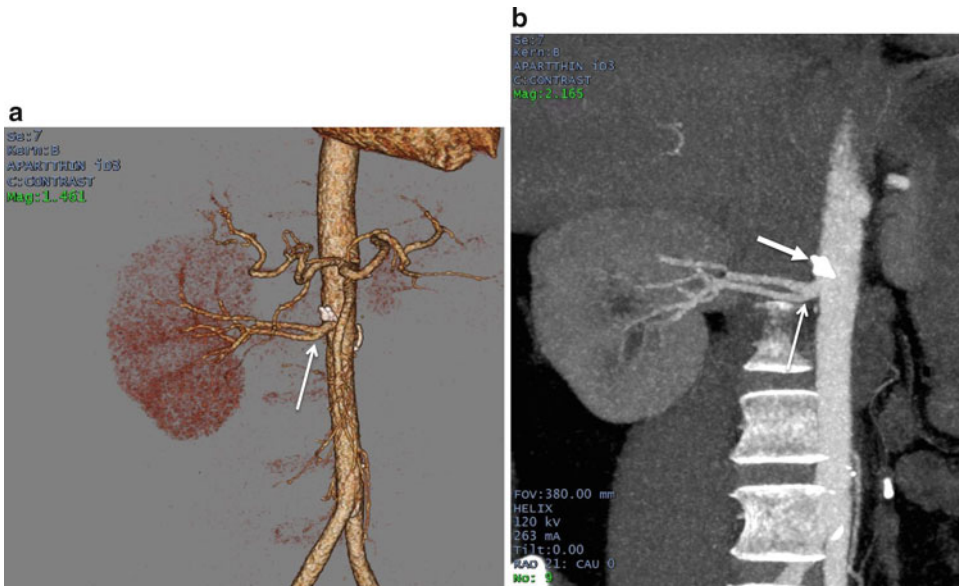
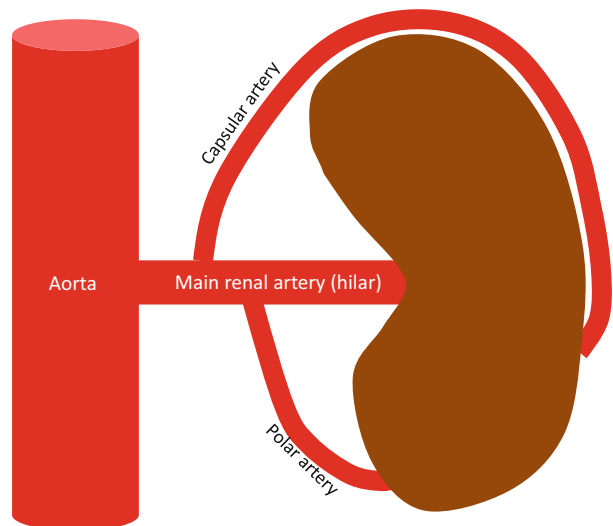


Fig. 7 Early renal artery branching. (a) 3D volume-rendered image from a CTA in a patient post left nephrectomy demonstrates a single right renal artery with an early bifurcation (arrow) just beyond the ostium. (b) The

corresponding maximal intensity projection image from the same CTA in a similar projection shows the early bifurcation (arrow) and adjacent surgical clips (thick arrow)

Fig. 8 Renal artery types



arteries perfusing the renal capsule are generally even smaller than polar arteries and course tangentially around, rather than into, the renal parenchyma. Capsular arteries generally perfuse little to no parenchyma and are ligated without consequence (Pozniak et al. 1998).

Intrinsic renal artery diseases affect the approach to renal donor harvesting. Atherosclerotic disease usually afflicts the origin and/or proximal segment of the main renal artery. Detecting significant atherosclerotic disease preoperatively may lead to intraoperative endarterectomy. Additionally, heavily calcified renal artery or aortic plaque threatens intimal laceration and life-threatening bleeding when clamped. Fibromuscular dysplasia (FMD) – a potentially stenosing arteriopathy – involves the mid and more distal renal arteries with a prevalence of 3.5–6% in living-renal donors (Edwards et al. 1992; Linder et al. 1989; Spring et al. 1979; Andreoni et al. 2002). CTA and MRA achieve sensitivity for FMD approaching 100% by demonstrating the “string-of-pearls” appearance, which refers to the alternating dilated and stenotic segments, along with focal stenoses and aneurysms involving the mid and/or distal renal artery and segmental arteries (Fig. 9). DSA secures the diagnosis in equivocal cases. Bilateral FMD contraindicates transplantation – unilateral FMD deserves circumspection and potentially venous grafting or other arterial reconstructive techniques (Balzer et al. 2007; Pfeiffer et al. 2002; Blondin et al. 2010).

Renal venous anatomy also plays into renal donor surgical planning, and CT and MRI demonstrate renal venous anatomy accurately. Renal venous anatomic variation occurs much more commonly than arterial variation (Pérez et al. 2013). The renal cortex drains successively into stellate, arcuate then interlobar veins, which anastomose, usually forming the superior and inferior venous trunks, which merge draining into the main renal vein, usually situated anterior to the artery at the renal hilum (Fig. 10). Multiplicity is more common in the right renal vein, present in 15–30% of the population (Harrison et al. 1978; Abrams 1983). However, the left renal vein often receives multiple tributaries along its longer

course to the IVC. A circumaortic configuration is the most common left-sided variant with a prevalence of 17% (Fig. 11) (Urban et al. 2001). The pre- and retroaortic limbs either arise from separate hilar veins or from a single hilar vein that splits before encircling the aorta. The left-sided retroaortic variant occurs in 3% of the population and usually courses caudally, draining into the lumbar IVC and less commonly the iliac vein (Kahn 1973; Chai et al. 2008; Kawamoto and Fishman 2006).

Renal venous measurements relevant to surgical planning include:

1. Right renal venous segmentary confluence to the IVC
2. Left renal venous segmentary confluence to the IVC
3. Left renal venous confluence to the left aortic margin

The lengths of the left and right renal veins average 8.5 cm and 2–2.5 cm, respectively (Cuttino and Clark 1990). The left kidney is favored because of the longer course of the left renal vein and, unlike the difficulty with the retrocaval arterial approach, transecting the left renal vein in front of the aorta is not problematic. However, unlike the right renal vein, the left renal vein receives numerous tributaries, including the adrenal, gonadal, hemiazygous, ascending lumbar, and lumbar veins. Large tributary veins (>5 mm) often require modifications to the standard surgical approach (Türkvtan et al. 2009).

Another reason to favor CT over MRI in the transplant donor workup is the superior sensitivity of CT for stones, which is virtually 100% (Smith et al. 1996; Fowler et al. 2002). MRI demonstrates the secondary findings of perinephric edema and periureteral edema vividly in the setting of obstructive urolithiasis, the sensitivity to non-obstructing renal stones is mediocre and much lower than CT (Sudah et al. 2001; Lipkin and Preminger 2013; Regan et al. 2005). The utility of CT lies in the fact that virtually all renal calculi attenuate X-rays much more than the surrounding renal parenchyma and all other tissues, with the exception of the skeleton (Figs. 2 and 12) (Saw

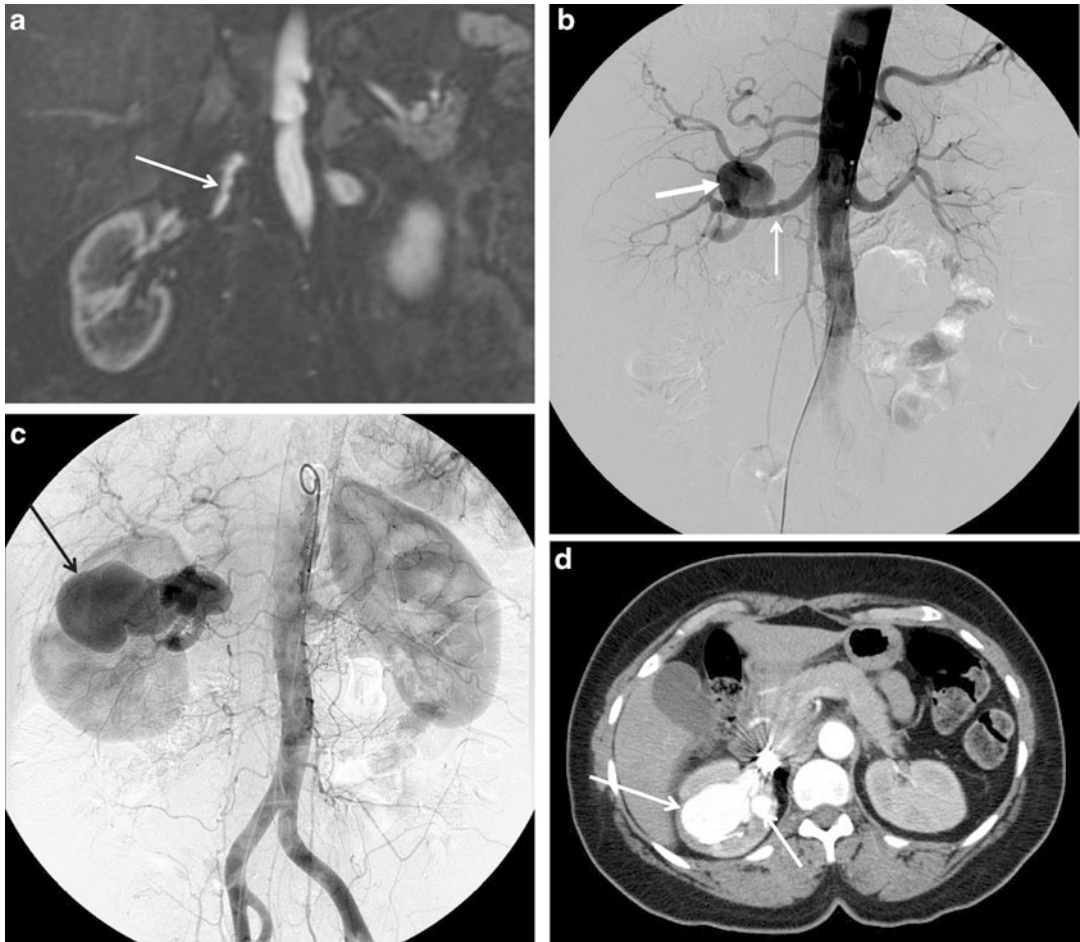


Fig. 9 CTA and MRA of fibromuscular dysplasia. **(a)** The T1-weighted, fat-suppressed postcontrast MRA image shows beaded irregularity of the right renal artery (*arrow*). **(b)** The image from a catheter-directed arteriogram also reveals the beaded appearance of the right renal artery (*arrow*) and an aneurysm arising from the right renal

artery (*thick arrow*). **(c)** A more delayed image from the arteriogram reveals another larger renal artery aneurysm (*arrow*). **(d)** The CTA image shows the renal artery aneurysms (*arrows*) demonstrating enhancement equivalent to the aorta

et al. 2000). Kidneys with small asymptomatic renal calculi (<4 mm) are safely harvested, while larger and symptomatic calculi require treatment (Martin et al. 2007).

CT and MRI detect renal masses with high sensitivity and relatively high specificity. Renal cysts are encountered very frequently and pose no barrier to transplantation (Grottemeyer et al. 2009). Cysts appear hypodense compared with normal renal parenchyma and exhibit no enhancement or complexity (i.e., mural nodularity or septation) (Fig. 13). While the appearance is unmistakable in larger lesions, with small size

(<15 mm), distinguishing cystic versus solid composition on CT is challenging because of “pseudoenhancement,” where an increase in lesion density following contrast administration is induced by artifactual phenomena, rather than true enhancement (Maki et al. 1999; Wang et al. 2008). Correlation with either US or MRI is useful because both modalities characterize small renal lesions accurately (Lingard and Lawson 1979; Einstein et al. 1995; Zagoria 2000; Ho and Choyke 2004; Nikken and Krestin 2007). Sonographically, simple cysts conform to spherical, uniformly anechoic (dark) lesions with

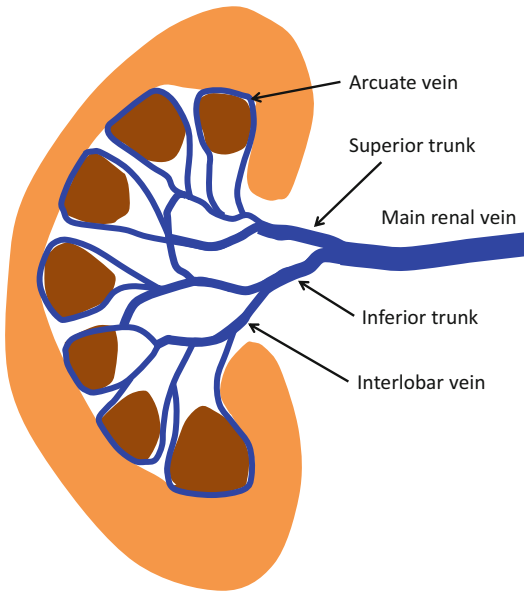


Fig. 10 Renal venous anatomy

acoustic enhancement (increased transmission of sound waves distally, which brightens tissues deep to the cyst) and a thin, barely perceptible wall. Simple cysts demonstrate marked hyperintensity matching other fluid-filled structures (i.e., gallbladder, thecal sac) on T2-weighted MRI images with corresponding T1-hypointensity and lack of enhancement (Fig. 13). When simple cysts are complicated by hemorrhage, infection, or inflammation, the imaging appearance changes. However, the common denominator of simple and complicated cysts is lack of vascular flow and enhancement. Sonographically, complicated cysts contents are hypoechoic (as opposed to anechoic) and/or septated, potentially with a thickened wall. Septation is also an occasional complicated cyst feature on CT and MR images and hemorrhagic or proteinaceous contents appear relatively CT hyperdense. Hemorrhage and protein convert

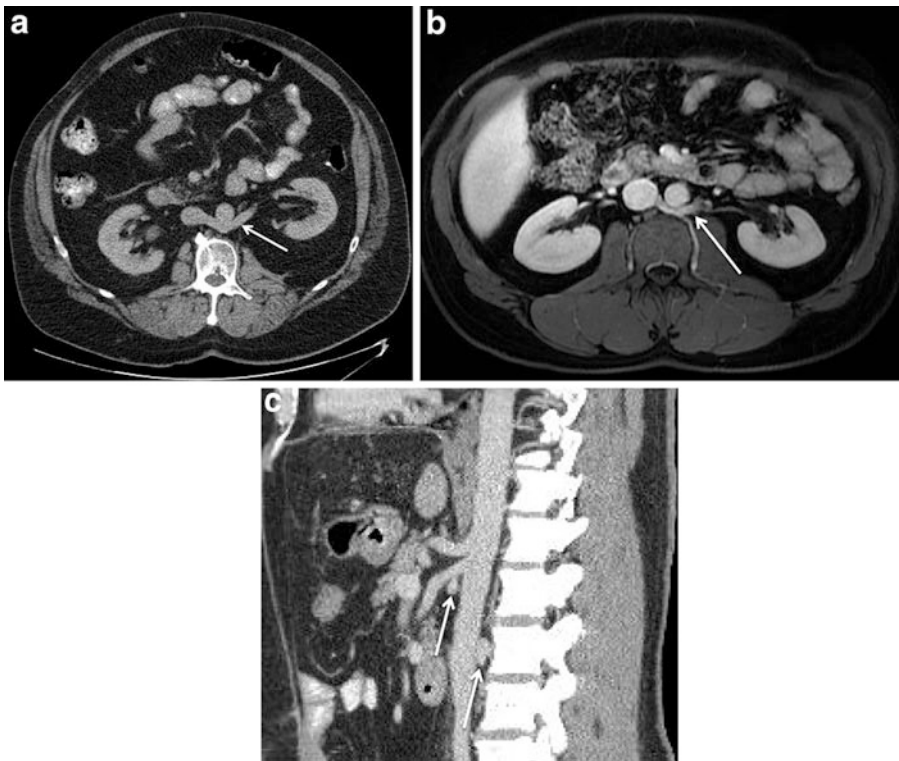


Fig. 11 Renal venous anomalies. (a) Axial postcontrast CT image shows a retroaortic left renal vein (*arrow*). (b) In a different patient, the T1-weighted, fat-suppressed post-contrast MR image shows a retroaortic limb (*arrow*) of a

circumaortic vein. (c) The sagittally reformatted image shows both limbs of the circumaortic left renal vein (*arrows*) surrounding the aorta

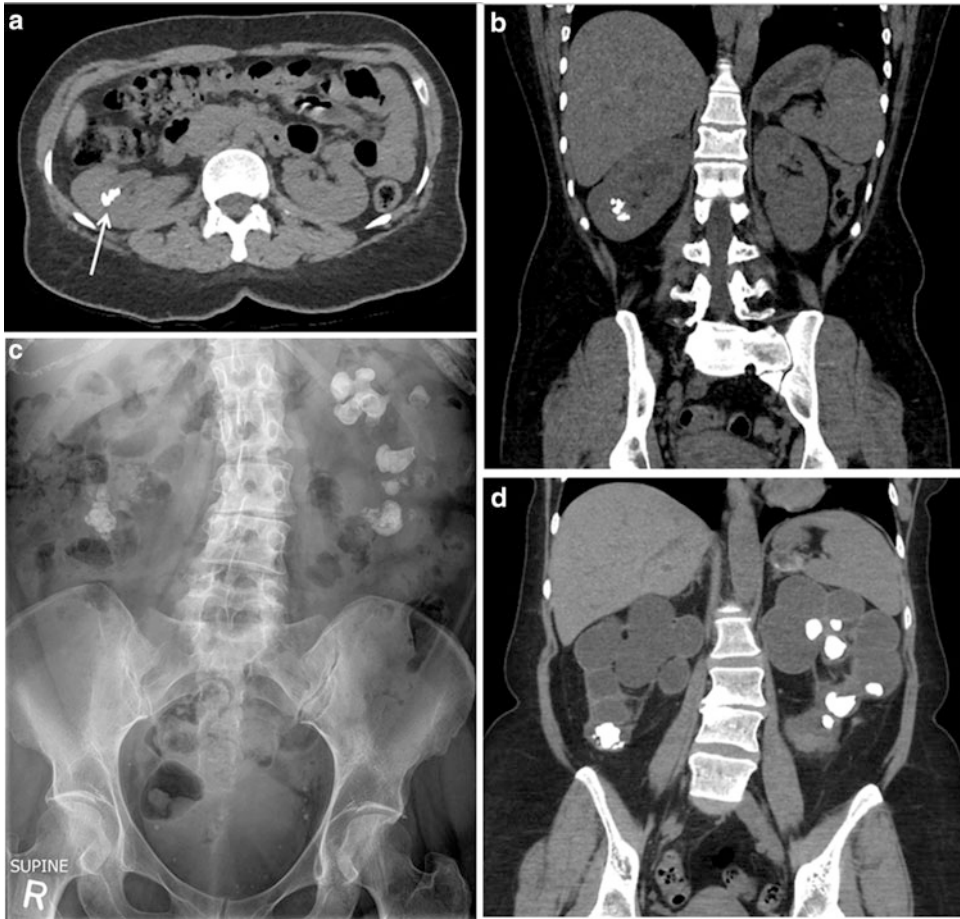


Fig. 12 CT of renal calculi. (a) Axial unenhanced CT image shows multiple calcified stones in the right renal collecting system (*arrow*) with no stones in the left kidney. (b) The coronally reformatted CT image shows the stones in the right renal lower polar collecting system and right renal hydronephrosis. (c) Supine X-ray in a different

patient reveals multiple large calcifications projected over the renal shadows bilaterally. (d) The corresponding coronally reformatted CT image shows the value of tomographic imaging by revealing the underlying polycystic renal disease, in addition to the renal calculi

simple fluid MR signal characteristics from T1-hypo- and T2-hyperintense to the opposite pattern – T1-hyper- and T2-hypointense with or without a fluid-fluid level (Fig. 13).

Neoplastic cysts must be differentiated from complicated nonneoplastic cysts because of the prognostic and management implications. Luckily, only a small minority of renal neoplasms appears truly cystic on imaging studies – approximately 10–15% (Koga et al. 2000; Harisinghani et al. 2003). The Bosniak renal cyst CT classification system was devised in an effort to standardize and stratify management based on the likelihood

of malignancy (Fig. 14) (Bosniak 1986; Curry et al. 2000; Siegel et al. 1997; Koga et al. 2000). The Bosniak classification system classifies renal cystic lesions from I to IV based on the degree of complexity. With increasing complexity – thicker septations, wall thickening, wall and/or septal enhancement – the risk of malignancy increases. With increasing malignancy risk, management escalates from none to imaging surveillance to ablative or surgical treatment.

The clear cell renal cell carcinoma (RCC) histologic subtype accounts for most renal cystic neoplasms, and 10–15% of RCCs are cystic

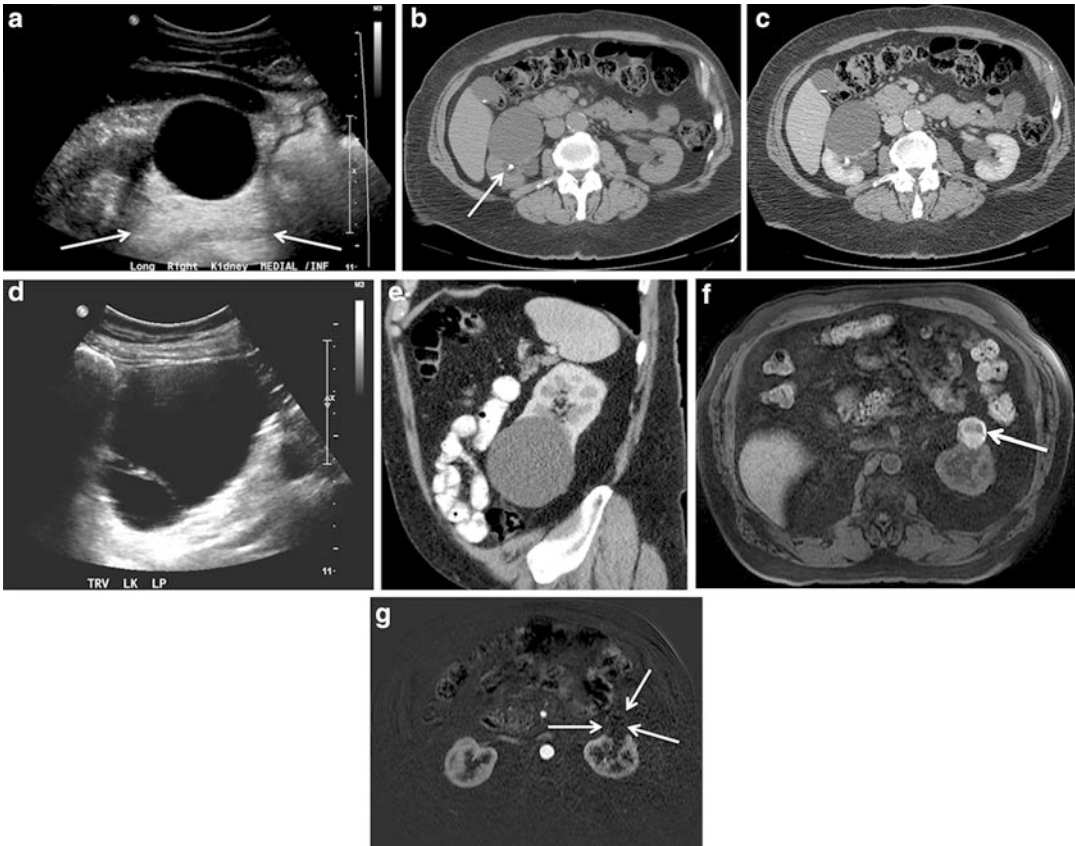


Fig. 13 Imaging of simple and complicated renal cysts. (a) Longitudinal sonographic image of the left kidney reveals a simple, unilocular, exophytic, uniformly anechoic cyst with acoustic enhancement (*arrows*) and an imperceptible wall. (b) The unenhanced CT image shows uniform fluid hypodensity within the cyst with an adjacent nonobstructing calculus (*arrow*). (c) The postcontrast CT image demonstrates absent enhancement within the cyst. (d) Transverse sonographic image in a different patient shows a large left renal cystic lesion with an irregular

thickened septation. (e) The corresponding sagittally reformatted postcontrast CT image demonstrates lack of enhancement, which relegates this cystic lesion to Bosniak Category IIF. (f) Axial T1-weighted, fat-suppressed MR image in a different patient reveals an exophytic lesion (*arrow*) arising from the left kidney with hyperintensity that indicates hemorrhage. (g) The postcontrast subtracted image reveals no enhancement within the lesion (*arrows*) confirming the cystic and nonneoplastic nature of the lesion

(Sun et al. 2009; Prasad et al. 2006). When even mostly cystic, cystic RCCs generally harbor perceptible enhancing nodules or septa or wall thickening and enhancement. The rare multilocular cystic RCC is the only consistently cystic RCC histologic subtype with a typical multilocular appearance with asymmetry of the intervening septa, simulating the multilocular cystic nephroma (MLCN). However, the demographic patterns diverge with the multilocular cystic RCC favoring males with a mean age of 51 and MLCN demonstrating a bimodal distribution – males

aged 3 months to 4 years and females in the 5th to 6th decades (Chowdhury et al. 2013; Freire and Remer 2009). Herniation into the renal pelvis is a distinctive feature of MLCN (Kettritz et al. 1996).

While cystic lesions only occasionally imply malignancy, solid lesions detected radiographically are generally malignant RCC (Silverman et al. 2008). The prevalence of solid benign lesions identified radiographically is fairly low – 12.8% in a series of 2770 cases – and oncocytomas and angiomyolipomas (AMLs) constitute most of the benign lesions. With smaller size, benignity

Category	Description	Imaging Features	Malignancy Risk	Management
I	Simple cyst	Imperceptible wall with fluid contents	0%	None
II	Minimally complicated cyst	Minimal septations without enhancement; thin calcifications	0%	None
IIF	Mildly complicated cyst	Mildly thickened septations; thickened or nodular calcifications	5%	Imaging surveillance
III	Complex cyst	Thickened or nodular septa or wall	55%	Ablation or partial nephrectomy
IV	Cyst with solid components	Enhancing soft tissue components	100%	Ablation or partial or total nephrectomy

Fig. 14 Bosniak classification of renal cystic lesions

becomes more likely: 25% <3 cm, 30% <2 cm, and 44% <1 cm (Frank et al. 2003). Small size also confers a relatively good prognosis for malignant lesions, especially when less than 3 cm (Rendon et al. 2000; Remzi et al. 2006). The only benign lesion diagnosed reliably on imaging studies is the AML due to its fat content. The AML typically appears hyperechoic sonographically because of its fat content and also hemorrhage and heterogeneous architecture (Raghavendra et al. 1983; Scheible et al. 1978; Lee et al. 1978; Bosniak 1981). While this appearance is suggestive, small RCCs often demonstrate increased echogenicity, which often prompts further evaluation with CT or MRI. CT and MRI demonstrate fat easily, as CT hypodensity less than water/fluid and MRI T1 and T2-hyperintensity suppressing with fat saturation (Fig. 15). The exception is the rare lipid-poor AML (representing 5% of cases), which simulates RCC (Yang et al. 2013; Sant et al. 1984; Jinzaki et al. 1997).

The appearances of other solid renal neoplasms generally overlap too frequently to confidently differentiate between them. As such, curative treatment—surgery or ablative techniques—is the standard for solid renal neoplasms detected radiographically. However, because with small size the frequency of benign neoplasms increases and the aggressiveness of RCCs decreases, conservative management with imaging surveillance

becomes more justifiable. Management strategies provide for imaging follow-up for lesions ranging from 1 to 3 cm. While RCC historically contraindicated transplantation, recent experience following partial nephrectomy offers promise (Ali et al. 2012; Meyyappan et al. 2012; Zhang et al. 2014). While lesion imaging patterns often differ, the features lack adequate specificity and enhancement on CT or MRI is the common denominator. Once a solid, enhancing renal lesion is identified, the next step in the imaging evaluation involves staging—assessing the renal veins and IVC for vascular invasion, the retroperitoneum for lymphadenopathy (lymph nodes greater than 1 cm in short axis diameter), and surrounding organs for metastatic spread.

Urinary tract disorders deserve attention because some contraindicate transplantation and others affect surgical planning. For example, hydronephrosis, papillary necrosis, medullary sponge kidney, and urothelial neoplasms contraindicate transplantation. Complete and partial ureteral duplication and ureteropelvic junction (UPJ) obstruction are important to detect and characterize presurgical planning. While ultrasound depicts pyelocalyceal distention in the setting of obstruction, identification, and characterization of other collecting system and ureteral disorders are better demonstrated on CT and MRI. Excreted contrast during the pyelographic phase after intravenous contrast administration (on both CT and MR

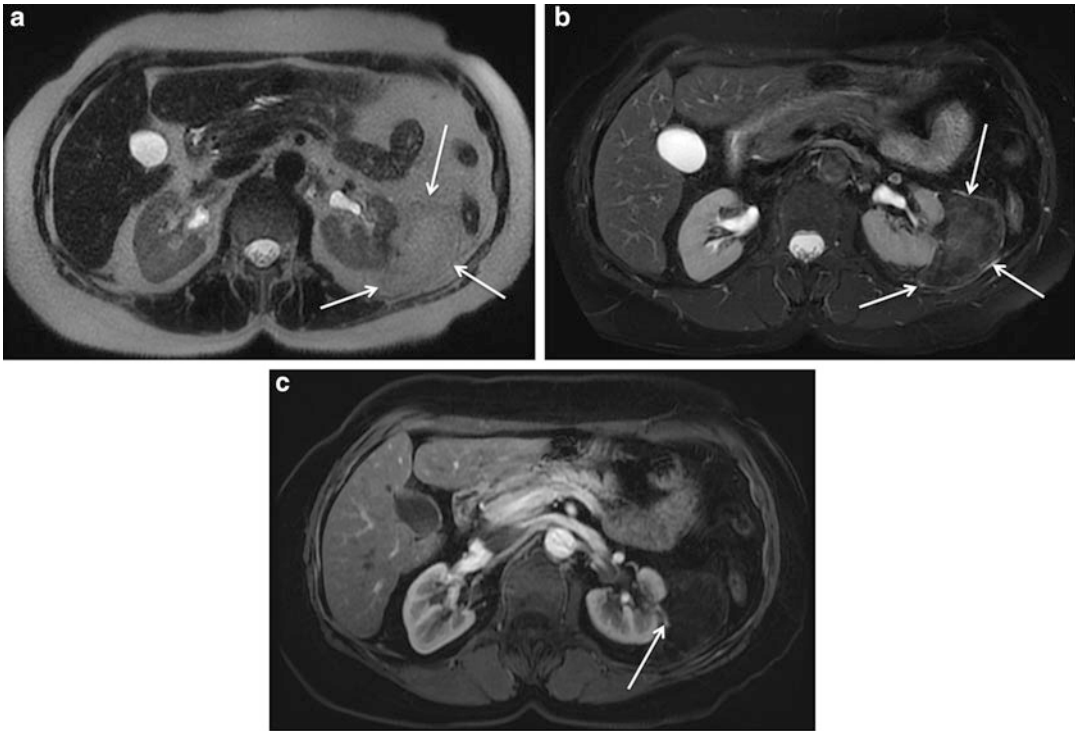


Fig. 15 Angiomyolipoma. (a) The axial T2-weighted image shows an exophytic lesion arising from the lateral aspect of the left kidney (*arrows*) with signal intensity matching retroperitoneal and subcutaneous fat. (b) The fat-suppressed T2-weighted image demonstrates virtual complete elimination of signal from the lesion (*arrows*)

confirming fat content and the etiology of angiomyolipoma. (c) The fat-suppressed, T1-weighted, arterial phase postcontrast image also reveals hypointensity equal to fat with a prominent, dysplastic arterial structure at the margin of the mass (*arrow*)

images) maximizes tissue contrast and offers the opportunity to postprocess image data and display the collecting system and ureteral anatomy with exquisite detail (Fig. 16). T2-weighted MR images also maximize collecting system and ureteral urine contrast and clearly demonstrate these conditions.

Renal Recipient Imaging

The indications for renal transplant recipient imaging are for: pretransplant screening and posttransplant complications. During the pretransplantation evaluation, the only routine imaging studies performed include a chest X-ray and screening mammography (within 12 months of transplant in women over 50 years of age). However, certain risk factors prompt a focused imaging

workup, specifically peripheral vascular disease (PVD) and cardiovascular disease (CVD). PVD – obviously common in this population – potentially complicates surgical technique because calcified plaque limits the ability to adequately clamp the vessel and threatens intimal laceration. Imaging screening options include either CT of the abdomen and pelvis without intravenous contrast to identify and quantify atherosclerotic calcification (especially of the iliac arteries) and CTA runoff to provide an assessment of the entire arterial system, depending on clinical findings (Fig. 17). Since cardiac disease is the leading cause of death following transplantation, CVD screening provides a means to improve posttransplant outcomes. Imaging screening is typically performed with either nuclear scintigraphy or echocardiography using either exercise or pharmacologic agents (if physical limitations preclude exercise).



Fig. 16 Collecting system duplication during the pyelographic phase. **(a)** Longitudinal sonographic image of the left kidney shows duplication of the collecting system with mild upper polar moiety hydronephrosis (*arrow*) and normal lower polar moiety collecting system (*thick arrow*). **(b)** The corresponding sagittally reformatted post-contrast CT image shows resolution of the upper polar moiety hydronephrosis (*arrow*) with normal appearance of the lower polar moiety. **(c)** Thick coronally reformatted CT image in the pyelographic phase postcontrast in a

different patient reveals a normal right renal collecting system and ureter and mild dilatation of the left lower polar moiety collecting system (*arrow*) with a small amount of contrast in the upper polar moiety collecting system (*thick arrow*). **(d)** The sagittally reformatted CT image through the left kidney shows layering excreted contrast in the upper polar moiety collecting system (*arrow*) and the distended lower polar moiety collecting system (*thick arrow*)

While renal transplant recipients undergo an extensive routine surveillance regimen, mammography and bone densitometry constitute the only surveillance imaging studies (Hariharan 2006). Screening mammography in these patients conforms to the standard annual recommendation for all patients. Bone densitometry is recommended

at the time of transplantation, at 6 months and annually if previous results are abnormal, otherwise every other year to monitor for the effects of steroid-induced bone loss (Fig. 18). Bone densitometry, or dual energy X-ray absorptiometry (DXA), estimates bone density by calculating the area density based on the X-ray attenuation

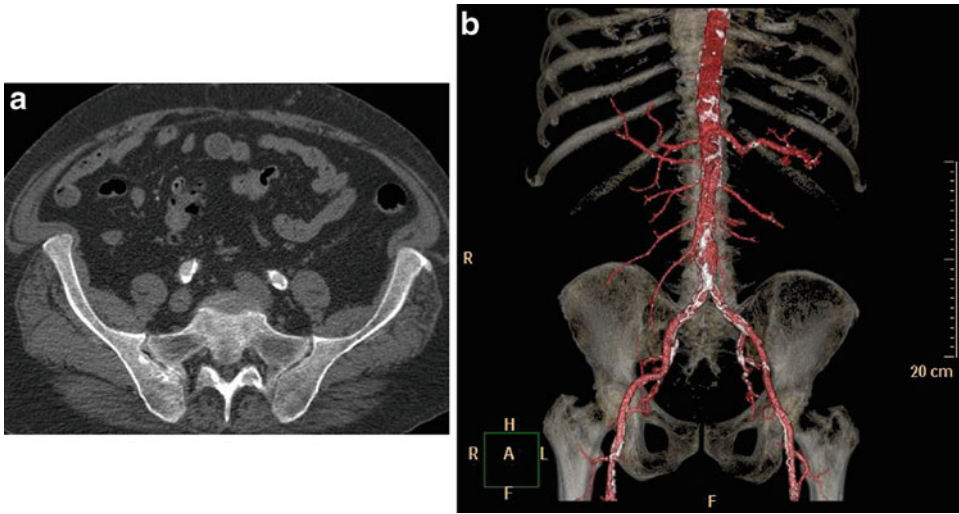


Fig. 17 CT and CTA in transplant recipient candidates. (a) The axial image from a CTA shows heavy atherosclerotic calcification of the common iliac arteries (*arrows*). (b)

The 3D volume-rendered image from the CTA shows the extent and distribution of atherosclerotic calcifications to better advantage

information obtained from two X-ray beams at different energies. The result is a calculated bone density in gm/cm^2 of regions-of-interest (ROIs) – typically the lumbar spine and proximal femurs and the distal radius is an alternative when other body parts are precluded by prior surgery or other condition. This number is compared to two cohorts – young adults and age-matched peers – to yield a T-score and Z-score, respectively, in standard deviation (SD) units. T-score value cut-offs for normal, osteopenia, and osteoporosis are: (1) -1.0 and higher = normal, (2) <-1.0 to -2.4 = osteopenia, and (3) ≤ -2.5 = osteoporosis. The FRAX[®] tool, developed by the World Health Organization (WHO), predicts the fracture risk integrating femoral bone density and clinical parameters, such as alcohol consumption, steroid use, history of fractures, tobacco use, etc., and is typically reported in terms of the 10-year probability of a major osteoporotic or hip fracture (Kanis 2016).

In the setting of graft dysfunction, imaging is generally implicated to help diagnose the etiology and to identify other potential complications. The long list of transplant complications stratifies according to postoperative time course, which limits the differential diagnosis considerably (Fig. 19). (Sharfuddin 2014) US, CT, MRI, and

nuclear medicine are the modalities generally implicated to evaluate graft dysfunction (Fig. 20).

Ultrasound

Ultrasound (US) usually is the initial imaging test (Fig. 20) because it is available, portable, able to provide anatomic and physiologic information, noninvasive, and avoids contrast material and ionizing radiation. It has no contraindications but may be technically difficult because of overlying bandages or surgery. Additionally, the superficial location of the graft allows higher frequency transducers and greater spatial resolution, which improve image quality.

The techniques used to evaluate renal transplants are grayscale (B-mode) ultrasound, as well as color Doppler and spectral Doppler. Grayscale ultrasound creates images from reflected sound waves and shows returning echoes as white or shades of gray. This method allows for evaluation of renal size and volume, renal parenchyma echogenicity, hydronephrosis, and peritransplant collections. The normal renal cortex is normally less or equally echogenic compared with the liver. The renal sinus is hyperechoic and the medullary pyramids mildly hypoechoic relative to

the renal cortex (Fig. 21). The shape of the allograft should be ellipsoid and the width should be greater than the anteroposterior dimension. Renal allograft hypertrophy is a ubiquitous finding that can be seen normally 6 months after transplantation, but is also present in acute rejection, pregnancy, or early diabetes mellitus (Absy et al. 1987).

Doppler ultrasound uses color encoding or spectral Doppler waveforms to display information about blood flow in the graft. Color flow shows direction and a gross estimate of vascularity (Fig. 22). Sensitive machines can show the main renal arteries (anterior and posterior divisions), segmental arteries, and some smaller arteries as well as their corresponding veins. Power Doppler is another mode where any blood flow is colorized but where arterial and venous flow are combined. This leads to better color filling in the

parenchyma. Spectral Doppler graphically displays flow and velocities accurately but from a small volume of tissue. The information is displayed as a spectral display with velocity in the y axis, time in the x axis, and amount of signal (roughly the number of red cells detected) as shades of white and gray. A useful parameter extrapolated from the spectral Doppler tracing is the arterial resistive index (RI). This is calculated by subtracting the end diastolic velocity (D) from the peak systolic velocity (S), that quantity divided by the peak systolic velocity (S) - [(S-D)/S]. A normal resistive index = 0.7–0.8; a resistive index greater than 0.75–0.8 is a non-specific indicator of transplant dysfunction (Rifkin et al. 1987). Resistive indices may be elevated in many processes, especially rejection, ATN, extrinsic compression from collections, and hydronephrosis.

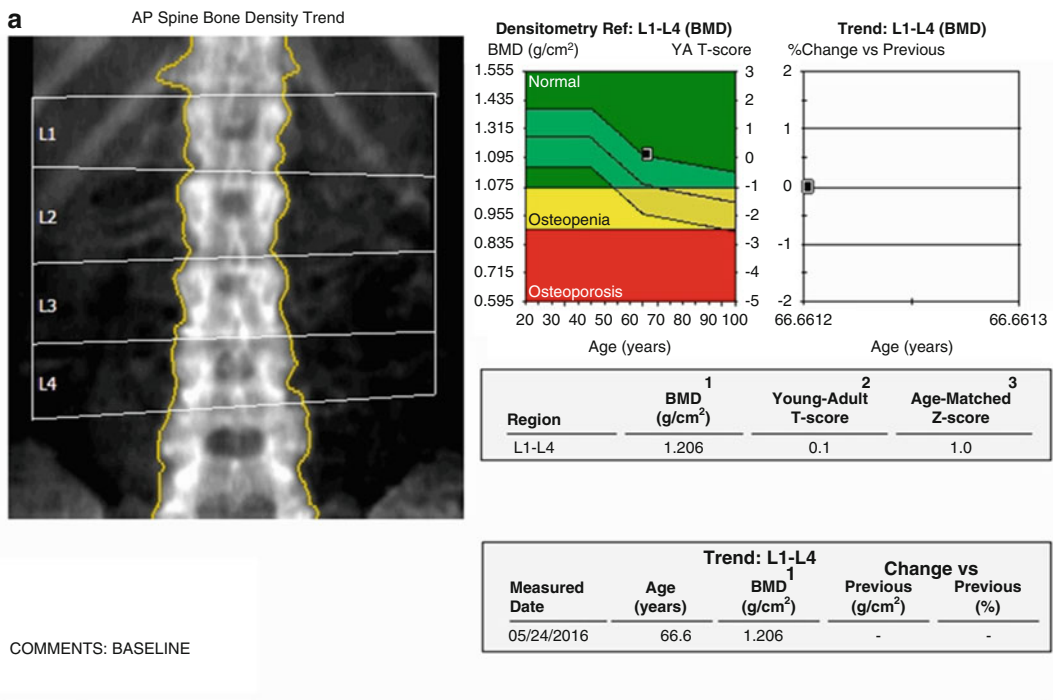


Image not for diagnosis
 Printed: 05/24/2016 12:02:10 PM (13.60)76:3.00:50.03:12.0 0.00:10.74
 0.60x1.05 17.8:%Fat=22.0%
 0.00:0.00 0.00:0.00
 Filename: g5to7o857q.dfx
 Scan Mode: Standard:OneScan 37.0 µGy

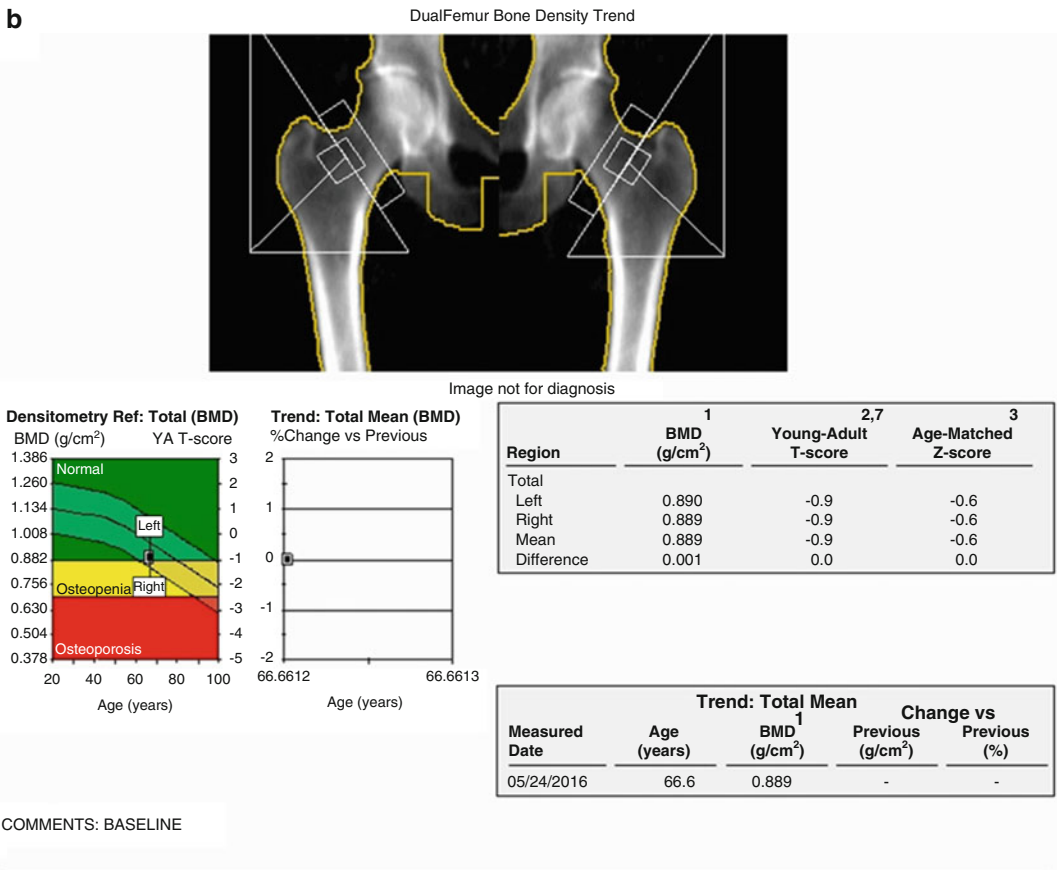
- 1 -Statistically 68% of repeat scans fall within 1SD (± 0.010 g/cm² for AP Spine L1-L4)
- 2 -USA (Combined NHANES (ages 20-30) / Lunar (ages 20-40)) AP Spine Reference Population (v112)
- 3 -Matched for Age, Weight (females 25-100 kg), Ethnic
- 11 -World Health Organization - Definition of Osteoporosis and Osteopenia for Caucasian Women: Normal = T-score at or above -1.0 SD; Osteopenia = T-score between -1.0 and -2.5 SD; Osteoporosis = T-score at or below -2.5 SD; (WHO definitions only apply when a young healthy Caucasian Women reference database is used to determine T-scores.)

Fig. 18 (continued)

The interpretation of the renal ultrasound should be made along with clinical, blood, and urinary findings. Interpretation also is affected by the time after transplantation, i.e., immediate (first week), early (one to 4 weeks), or late (after 4 weeks).

Immediate evaluation of graft function after transplantation is standard of care and correlates with shorter hospital stays and improved short-term and long-term survival (Ferguson and Henry 1993). Critical immediate complications are frequently vascular and can be diagnosed via duplex ultrasound. Arterial occlusion typically occurs at

the arterial anastomosis and there will be absence of arterial flow on Doppler. If equivocal or technically challenging, angiography, CT or MR, may be confirmatory. On gray scale, ultrasound findings of renal vein thrombosis are graft hypertrophy yielding an overall hypoechoic appearance and rarely a hyperechoic thrombus in the main renal vein. On Doppler, there is a characteristic reversal of diastolic flow on arterial spectral tracings (Fig. 23). The main renal vein is not seen if renal vein thrombosis is complete but can have an attenuated signal if part of the obstructed venous system remains open.



1 . Statistically 68% of repeat scans fall within 1SD (± 0.010 g/cm² for Dualfemur Total)
 2 . USA (Combined NHANES (ages 20-30) / Lunar (ages 20-40)) Femur Reference Population (v112)
 3 . Matched for Age, Weight (females 25-100 kg), Ethnic
 7 . DualFemur Total T-score difference is 0.0. Asymmetry is None.
 11 . World Health Organization - Definition of Osteoporosis and Osteopenia for Caucasian Women: Normal = T-score at or above -1.0 SD; Osteopenia = T.score between -1.0 and -2.5 SD; Osteoporosis = T-score at or below -2.5 SD; (WHO definitions only apply when a young healthy Caucasian Women reference database used to determine T-scores.)

Fig. 18 (continued)

c DualFemur FRAX*

Risk Factors:

- None
- Alcohol (3 or more units per day)
- Family Hist. (Parent hip fracture)
- Glucocorticoids (Chronic)
- History of Fracture (Adult)
- Secondary Osteoporosis
- Rheumatoid Arthritis
- Tobacco User (Current Smoker)

10-year probability of Fracture: ¹⁷

Major Osteoporotic ¹⁸	4.8%
Hip	0.7%
Population	USA (Black)
Based on DualFemur (Left) Neck BMD	

*FRAX is a trademark of the University of Sheffield Medical School's Centre for Metabolic Bone Disease, a World Health Organization (WHO) collaborating Centre.

COMMENTS: BASELINE

Printed: 05/24/2016 12:02:22 PM (13.60); Filename: g5to7o857q.dfx; Right Femur; 17.6%Fat=26.9%; Neck Angle (deg)= 57; Scan Mode: Standard 37.0µGy; Left Femur; 17.7%Fat=26.9%; Neck Angle (deg)= 57; Scan Mode: Standard 37.0µGy
FRAX v3.1

17 - The 10-year probability of fracture may be lower than reported if the patient had received treatment.

18 - Major Osteoporotic Fracture: Clinical Spine, Forearm, Hip or Shoulder

Fig. 18 Bone densitometry. (a) Dual-energy image of the lumbar spine is obtained, and ROIs are manually generated to isolate L1–L4 vertebral bodies and individual vertebral body bone densities are generated from which a composite bone density in grams per centimeter squared is calculated, which corresponds to a T-score. The T-score represents bone density compared with the normal young adult bone

density in standard deviations (−1.0 and above = normal, −1.1 to −2.4 = osteopenia, <−2.5 = osteoporosis). (b) Bilateral proximal femoral bone density is also measured with T-scores generated in the same fashion. (c) The fracture assessment tool (FRAX) uses bilateral femoral bone densities in conjunction with clinical parameters to predict the risk of osteoporotic fracture

Diagnosing acute tubular necrosis can be difficult and often has overlapping findings with accelerated acute rejection and acute rejection. Furthermore, the grafts can appear normal on ultrasound in biopsy proven disease. Potential findings include hypertrophy with a generalized hypochoic appearance and loss of normal cortical and medullary differentiation. The resistive index may be elevated in acute tubular necrosis or can be normal.

The sonographic appearance of accelerated acute rejection is hypertrophy from edema, hypochoic cortex, swelling of the medullary pyramids, loss of corticomedullary differentiation, and edema in the renal sinus fat. In severe cases Doppler can show reversed diastolic flow and elevation in the resistive index. These findings are identical to acute tubular necrosis and acute rejection as mentioned previously.

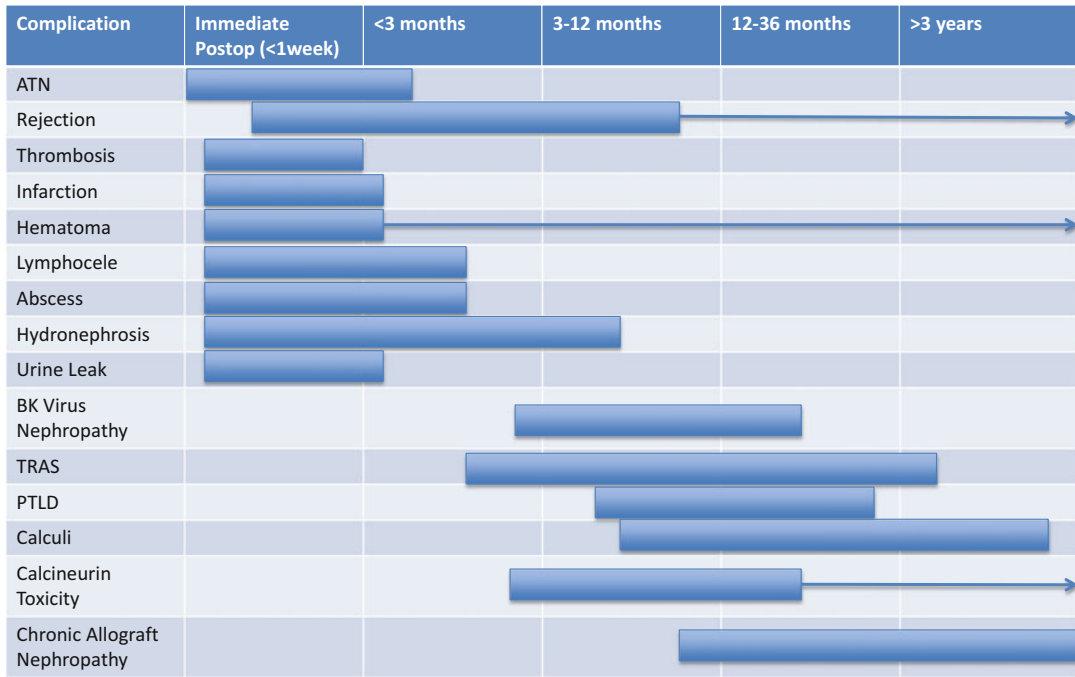


Fig. 19 Postoperative renal transplantation complications

Complication	US	CT	MRI	NM	DSA
Early postoperative dysfunction/ATN	1 st -line; operator-dependent; detects hydronephrosis and collections	NA	NA	2 nd -line; not readily available; time-consuming	NA
Urinary tract obstruction	1 st -line; follow serially for improvement	2 nd -line; sensitive for calculi and other potential obstructing lesions	NA	2 nd -line; differentiate functional from chronic obstruction	NA
Renal artery stenosis	1 st -line; operator-dependent	Theoretically high accuracy; risk of nephrotoxicity	2 nd -line; confirmatory after US; gadolinium contraindicated with eGFR <30	NA	2 nd -line; confirmatory; simultaneous intervention; risk of nephrotoxicity and procedure complications
Fluid collections	1 st -line; follow serially; option for simultaneous drainage	2 nd -line; anatomic depiction; surgical planning	3 rd -line; problem-solve equivocal cases	Only useful for possible urine leak	NA
PTLD	2 nd -line	1 st -line; sensitive; nonspecific	1 st -line; sensitive; nonspecific	NA	NA
Nephrolithiasis	2 nd -line; follow serially	1 st -line; sensitive and specific	NA	NA	NA
Biopsy complications	1 st -line	2 nd -line	NA	NA	2 nd -line; sensitive and specific; simultaneous intervention; risk of nephrotoxicity and procedure complications

Fig. 20 Imaging modalities and transplant complications

Fig. 21 Ultrasound image of normal renal transplant. (a) The longitudinal gray-scale ultrasound image of the renal allograft in the left iliac fossa demonstrates the normal hypoechoic appearance of the renal cortex (*arrows*) compared with the echogenic renal sinus (*thick arrow*). (b) The longitudinal gray-scale ultrasound image of renal allograft a few days after transplant shows the hypoechoic medullary pyramids to better advantage (*arrows*)



Other complications that can occur in the immediate posttransplantation period are acute tubular necrosis (ATN) and accelerated acute rejection. ATN gray scale findings are usually absent but may demonstrate hypertrophy with a generalized hypoechoic appearance and loss of normal cortical medullary differentiation. Arterial RIs may be normal or elevated.

The sonographic appearance of acute rejection is enlargement of the transplant especially anterior-posterior with respect to width giving a round cross-sectional shape. Hypertrophy from edema, hypoechoic cortex, swelling of the medullary pyramids, loss of corticomodullary differentiation, and edema in the renal sinus fat may be found. In severe cases Doppler can show elevation in the resistive

index or even absent or reversed diastolic flow. These findings may be identical to acute tubular necrosis; acute rejection may require biopsy, response to therapy, or progression or regression over time to distinguish between the two.

Hematomas can be a normal posttransplant finding following surgery and typically appear as fluid collections, sometimes with complex internal architecture and septations (Fig. 24). Hematomas are frequently anechoic immediately and after the liquefaction. More commonly, the fluid has some or many internal echoes, sometimes with septations. Abscesses are rare but demonstrate fluid with echoes. If characterization of peritransplant fluid is required, ultrasound-guided aspiration is usually easy due to the superficial position

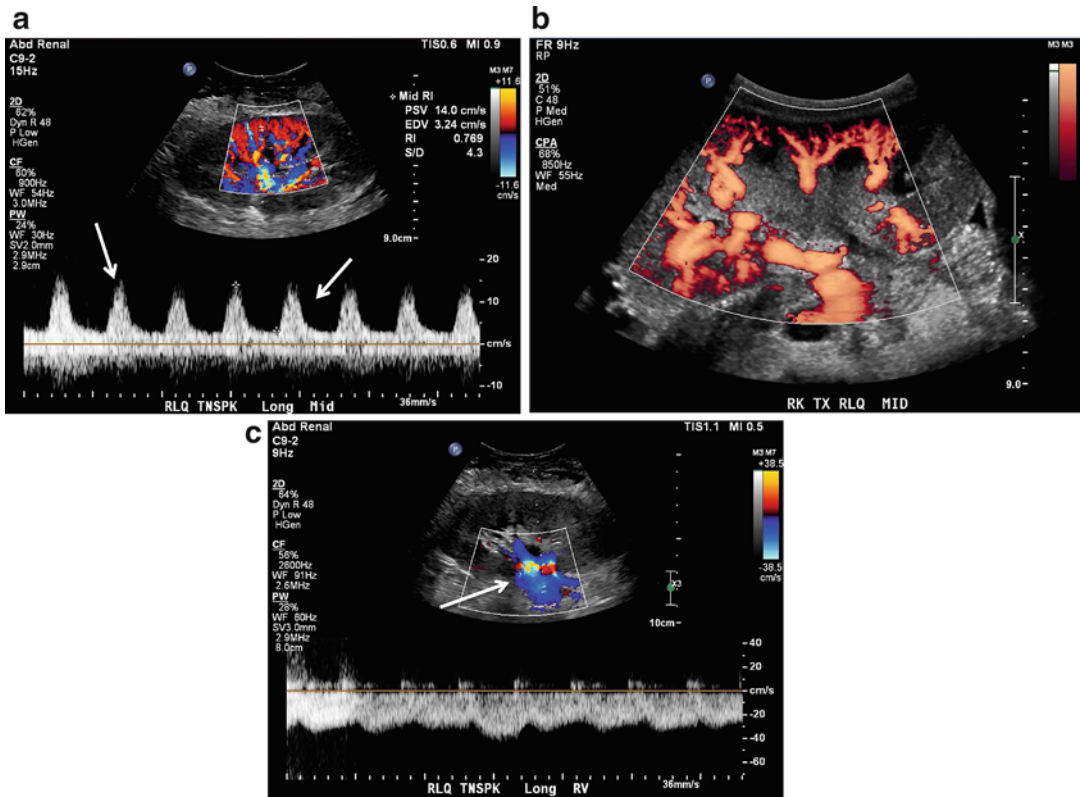


Fig. 22 Normal color and spectral Doppler images in renal transplantation. **(a)** Color Doppler image shows how blood flow is color-encoded depending on whether flow is toward (*red*) or away from (*blue*) the ultrasound probe. Additionally, a spectral Doppler tracing (*arrows*) can be obtained from a selected vessel in order to assess hemodynamics, such as the resistive index (*asterisk*),

which in this case is normal. **(b)** The power Doppler image demonstrates the magnitude of flow without the directionality. **(c)** Color Doppler is also used to demonstrate the patency and flow characteristic of the major renal vessels, and this example shows the normal renal vein with blood flow directed away from the allograft (*arrow*) with the spectral waveform showing normal velocity

of the graft. Fluid collections such as hematomas rarely cause sufficient mass effect to alter hemodynamics. Ascites adjacent to the graft does not have the well-defined wall fluid collections do.

Early complications (occurring at 1–4 weeks) are acute rejection, urinary fistula, and ureteral obstruction. Acute rejection was originally described with typical gray-scale findings. These are frequently minimal or absent as treatment for rejection has improved so dramatically. Enlargement rounding and equalization of the anteroposterior dimension and width, hypoechoic cortex, swelling of the medullary pyramids, loss of corticomedullary differentiation, thick uroepithelium, and diminished echogenicity in the renal sinus fat have been described.

Hydronephrosis usually indicated ureteral obstruction. Attention to the ureterovesical anastomosis on ultrasound is important as this is the most common site of obstruction, urinary leak, or narrowing. Intrinsic narrowing can be caused by fibrosis, ischemia, blood clots, or rejection. Ultrasound of the ureter may show internal echogenic contents or diminished caliber of the ureter. Examples of extrinsic secondary causes of obstruction are fluid collections. Ureteral reflux can cause hydronephrosis but is uncommon compared with obstruction.

Large urinary fistulas or leaks commonly occur at the ureterovesical junction and present with urinomas and/or urinary ascites. Urinomas appear as hypoechoic fluid collections, internal

Fig. 23 Renal vein thrombosis. The renal arterial spectral Doppler tracing shows transient diastolic flow reversal (arrow), which is a nonspecific finding of graft dysfunction

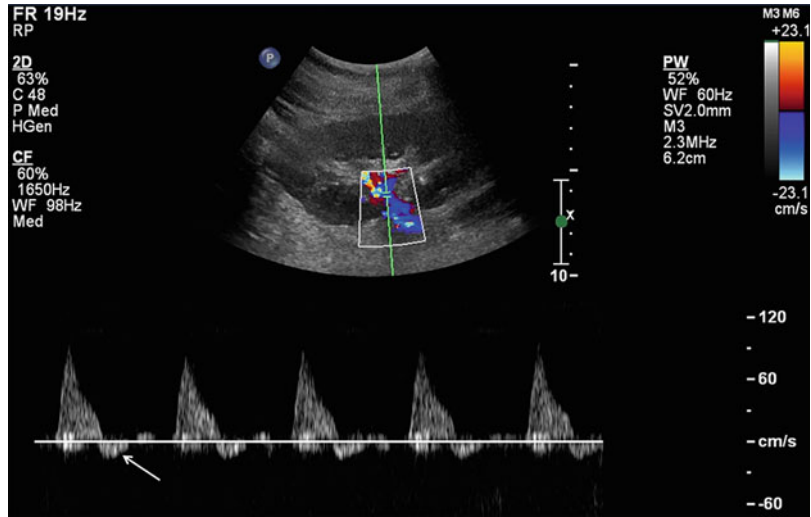
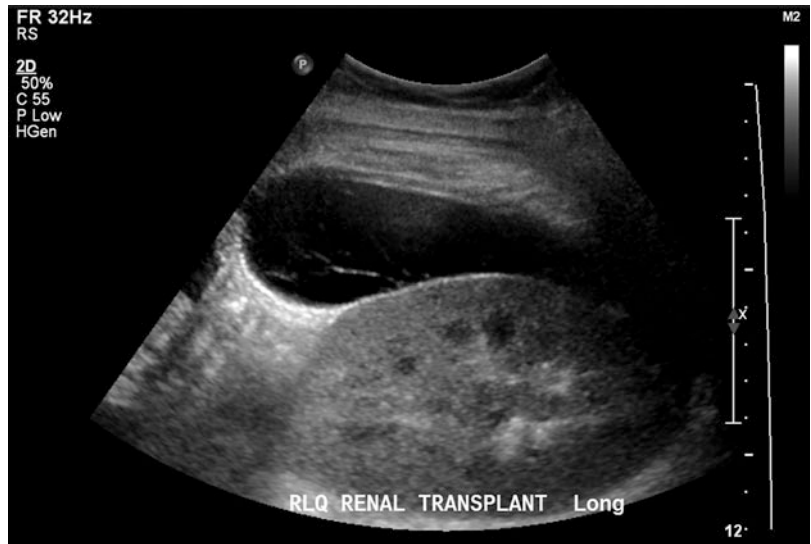


Fig. 24 Posttransplant hematoma. Hypoechoic collection superficial to the kidney containing internal septations



septations are less often seen compared with hematoma so (Fig. 24). Diagnosis can be confirmed with ultrasound guided percutaneous needle sampling of the fluid or opacification of the collection after contrast administration.

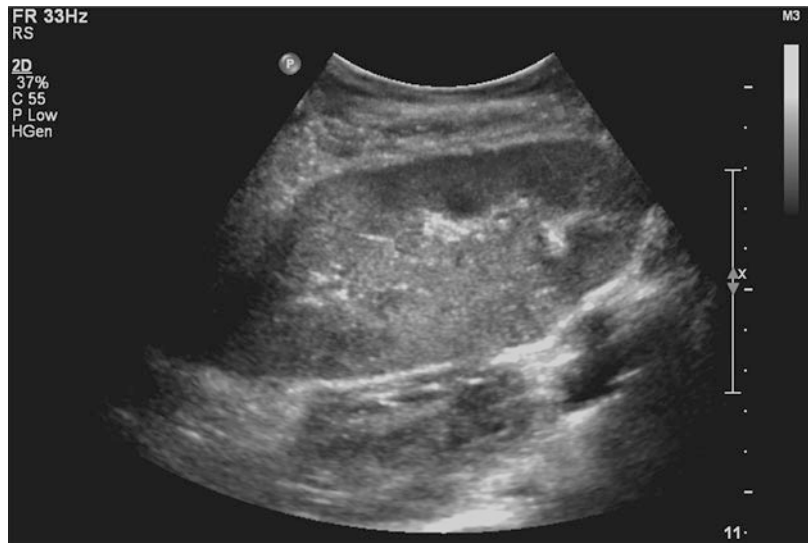
Late complications after transplantation include chronic rejection, collections and infections, vascular processes, and posttransplant lymphoproliferative disorder (PTLD). PTLD can appear as focal hypoechoic solid masses in or around the renal parenchyma.

Chronic rejection is seen as atrophy and thinning of the renal cortex. Other potential findings

include increased echogenicity (Fig. 25) and a decreased number of intrarenal vessels (Bin et al. 2007). On spectral Doppler, the RI is normal to slightly elevated.

Lymphoceles are collections of lymphatic fluid that appear as round fluid collections, the fluid lacking internal echoes. The kidney with pyelonephritis may appear normal or enlarged. There may be focal hypoechoic regions. Color may show reduced cortical vascularity. There may be echogenic debris in the collecting system and/or thickening of the uroepithelium. Abscesses are fluid collection in or around the

Fig. 25 Chronic rejection. Longitudinal gray-scale US of a renal allograft placed years earlier shows increased cortical echogenicity in the setting of histopathologic findings of chronic rejection



transplant, the fluid usually has low level echoes.

Renal artery stenosis commonly occurs at the anastomosis. Doppler ultrasound will show high velocity at the site of narrowing. Downstream turbulence is detected beyond the high velocity jet. Diminished RI and/or accelerations in the parenchymal vessels are also specific findings but are less sensitive than the direct evaluation of the transplant artery itself. Doppler criteria for renal artery stenosis are an elevated renal artery peak systolic and/or an elevated ratio of blood velocities in the stenotic renal artery divided by the iliac artery. Intrarenal waveforms are frequently blunted. An iliac inflow stenosis can create similar pathophysiology with blunted intrarenal waveforms without the elevated velocities in the main artery.

Arteriovenous fistulas (AVFs) can result from biopsy or rarely from surgical technique. Asymmetrically enlarged arteries and draining veins are often seen with larger AVFs on color. The turbulence that AVFs create are common and produce false color in the parenchyma (“color bruit artifact”) and heralds an underlying vascular process (Fig. 26). Arterial feeders show increased arterial systolic and diastolic velocities and the draining vein can show pulsatile (“arterialized”) flow.

Pseudoaneurysms may form as a result of biopsy, rarely from surgical technique or infection.

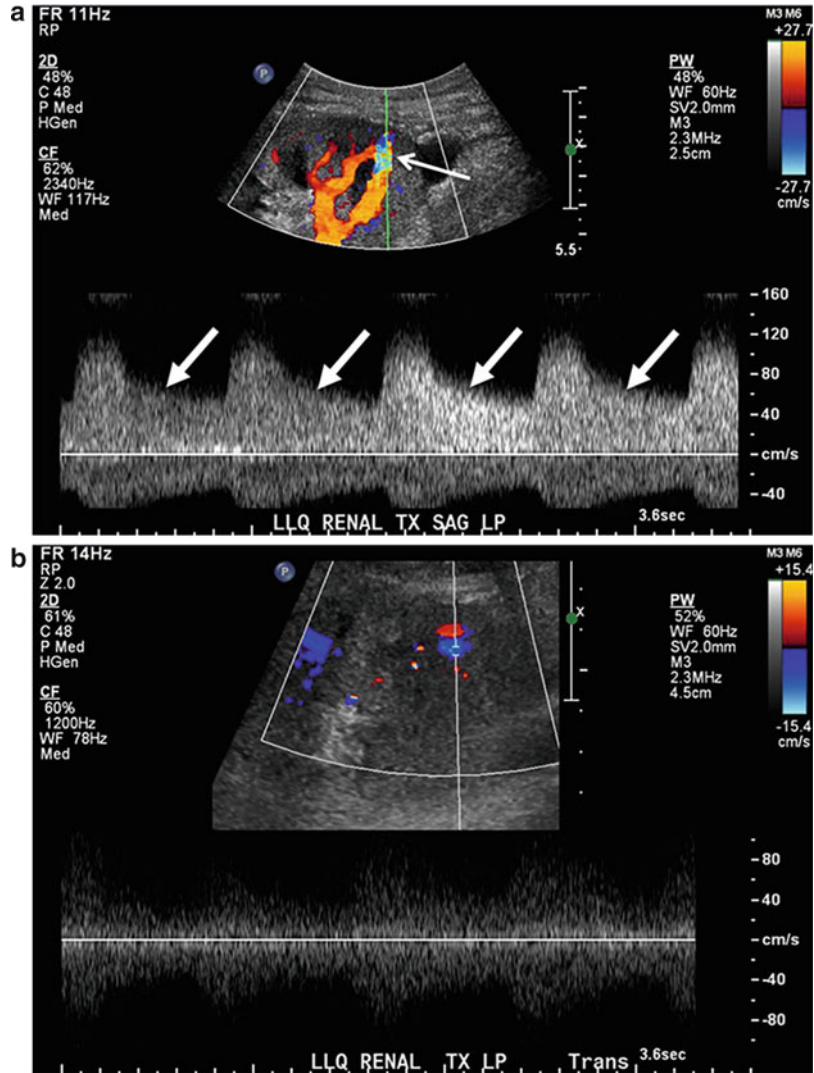
Pseudoaneurysms appear as round hypoechoic areas with internal color flow. All “cysts” in the transplant should be evaluated with color since pseudoaneurysms may mimic masses or cysts. Doppler is used to diagnose pseudoaneurysms. In addition to the color flow in the collection, the pseudoaneurysm neck can be identified and typical spectral Doppler “to-and-fro” flow into and out of the pseudoaneurysm sac are definitive.

Hydronephrosis can be detected at any time frame from transplantation but is not always significant obstruction (Fig. 27). A dilated collecting system can occur due to reflux across an incompetent ureteroneocystostomy or a denervated flaccid collecting system. These can often be distinguished from obstructive hydronephrosis by having the patient void (Koga et al. 1996; Platt et al. 1989; Platt et al. 1991).

CT

CT plays a secondary role in imaging post-transplant complications. While providing a useful anatomic overview – albeit somewhat limited by the avoidance of iodinated contrast material in the setting of renal graft dysfunction – CT images lack the physiologic information that Doppler US provides. The normal CT appearance of the transplanted renal graft in the iliac fossa simulates the

Fig. 26 Arteriovenous fistula in the lower pole of the renal allograft in the left iliac fossa. **(b)** The spectral Doppler tracing of a prominent vessel at the lower pole of the renal allograft (*arrow*) demonstrates relatively elevated diastolic flow velocities (*thick arrows*) indicating low resistance in the setting of a direct arterial-venous communication. **(b)** The corresponding venous waveform reveals pulsatile flow



appearance of native kidneys, except for mild collecting system dilatation due to ureteral anastomotic edema (Muglia et al. 2013). In the immediate posttransplant setting, changes in the fat surrounding the renal transplant are inevitably present, including small fluid collections, which often appear heterogeneously dense because of blood content (Fig. 28). Unless associated with mass effect on adjacent structures, signs of infection, or urinary complications, fluid collections in the immediate postoperative period are considered incidental and typically followed with US. One notable exception is a hematoma in the setting of potential graft rupture or vascular pedicle

injury (Sebastià et al. 2001). However, hematomas generally do not signify catastrophic complications and appear relatively hyperdense compared with simple fluid in the acute phase and undergo a progressive decline in density with evolution of blood products and gradually decrease in size.

CTA serves an ancillary role in assessing post-transplant vasculature due to the need for iodinated contrast and its potential nephrotoxicity. While US is the first-line diagnostic test, CT plays a problem-solving role when MRI is precluded by susceptibility artifact (signal void obscuring regional structures) arising from

Fig. 27 Hydronephrosis in transplanted renal allografts. **(a)** Longitudinal gray-scale US image of a renal allograft in the left iliac fossa shows a branching anechoic, fluid-filled structure corresponding to mild hydronephrosis. **(b)** Longitudinal gray-scale US image in a different patient with a right iliac fossa renal allograft shows a greater degree of collecting system, pelvic, and proximal ureteral distention connoting moderate hydronephrosis



surgical clips or other foreign bodies or implanted devices (Hofmann et al. 1999). Renal artery stenosis, the most common vascular complication, usually occurs near or at the anastomosis and appears as a narrow waist measuring less than 50% of the caliber of the prestenotic normal vessel (Eriksson et al. 2010).

CT also identifies other vascular complications, including renal artery thrombosis, iliac artery stenosis, arteriovenous fistula (AVF), pseudoaneurysm, and renal vein thrombosis and stenosis. Renal artery thrombosis occurs in the immediate transplant period and CTA demonstrates absent arterial enhancement and lack of

renal parenchymal enhancement (Fig. 29). AVFs and pseudoaneurysms usually arise following percutaneous biopsy and often resolve spontaneously. Both lesions usually appear as round arterially enhancing lesions with AVFs demonstrating early venous drainage. Renal vein thrombosis also requires intravenous contrast administration, but with a longer delay to opacify systemic veins. Findings range from a discrete hypodense filling defect against enhancing normal venous lumen to complete lack of enhancement. Venous stenosis is seen on CT images as a significant caliber luminal caliber change usually in the perianastomotic region.



Fig. 28 CT of posttransplant fluid collections. (a) The precontrast image shows an ovoid fluid collection (*arrow*) medial to the renal allograft in the right iliac fossa (*thick arrow*). (b) The corresponding postcontrast image demonstrates absent enhancement, confirming the absence of solid tissue and the cystic nature of this

lymphocele. (c) An axial unenhanced image in a different patient reveals a large, heterogeneous collection (*arrows*) surrounding a renal allograft in the right iliac fossa (*thick arrow*). (d) The corresponding coronally reformatted image shows the extent of the large hematoma (*arrows*) surrounding the renal allograft (*thick arrows*)

Posttransplant urologic complications include urinoma and ureteral obstruction. The CT appearance of a urinoma is a nonspecific, hypodense fluid collection interchangeable with the appearances of seromas, lymphoceles, and chronic hematomas after the lysis of hyperdense blood products. The definitive CT diagnosis of a urinoma requires the intravenous administration of iodinated contrast material to confirm the communication from renal collecting system or ureter to the collection. Ureteral obstruction is easily identified as collecting system dilatation.

Immunocompromised-related posttransplant malignancies include skin, cervical, and rectal malignancies and Kaposi's sarcoma and lymphoma (Kyllönen et al. 2000). While PTLD frequently manifests with lymphadenopathy, PTLD potentially involves any organ, yet has a predilection for the transplanted renal graft (Lopez-Ben et al. 2000). Contrast-enhanced CT is generally the first-line imaging modality for PTLD because of its availability and diagnostic utility. Nodal disease involves any lymph node station and manifests as either: (1) a discrete, enlarged lymph

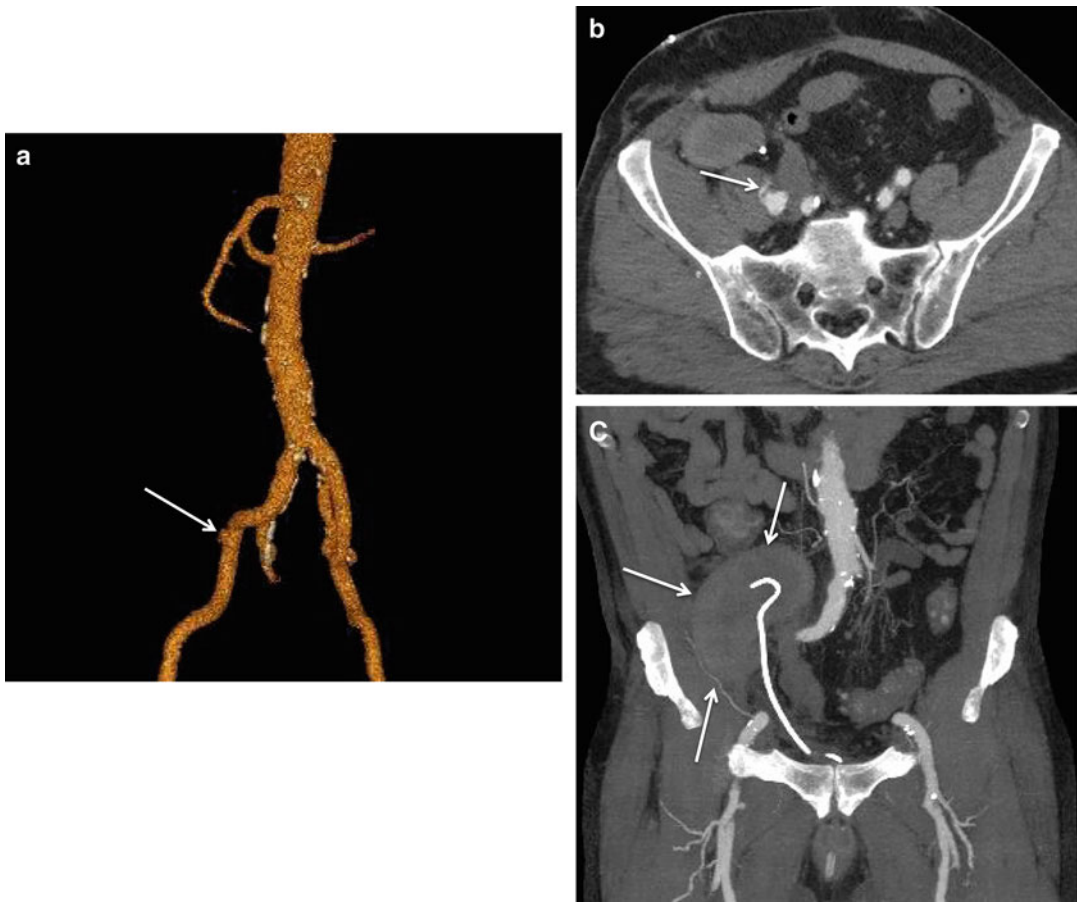


Fig. 29 Renal artery thrombosis. (a) Volume-rendered image from a CTA shows absence of the renal artery supplying the right renal allograft – only irregularity at the ostium is apparent (*arrow*). (b) Axial image from the

CTA shows an attenuated stump on the origin of the renal artery (*arrow*). (c) Coronal maximal intensity projection from the CTA shows minimal enhancement of the renal allograft (*arrows*)

node, (2) a cluster of enlarged lymph nodes, or (3) a bulky soft tissue with or without central necrosis (Fig. 30) (Borhani et al. 2009). PTLD involving the renal allograft generally conforms to either a homogeneous hilar mass or multifocal parenchymal masses exhibiting relatively mild enhancement.

Positron emission tomography (PET)/CT combines the sensitivity for hypermetabolism characteristic of neoplastic tissue with the anatomic detail provided by CT. PET detects the radiation emitted by the decay of the glucose metabolism radiotracer 2-[fluorine-18]fluoro-2-deoxy-D-glucose (FDG). The PET/CT sensitivity and specificity for PTLD is greater than CT alone (Fig. 31)

(Borhani et al. 2009; Bakker et al. 2006; Bakker et al. 2007; Bianchi et al. 2008; McCormack et al. 2006). In addition to increasing the sensitivity for neoplastic lesions, PET/CT also adds utility in evaluating the response to therapy by demonstrating the posttreatment impact on metabolic activity, in addition to demonstrating size changes (von Schulthess et al. 2006).

MRI

MRI also plays an ancillary role in the post-transplant setting. However, MRI poses no risk to the allograft, involves no ionizing radiation,

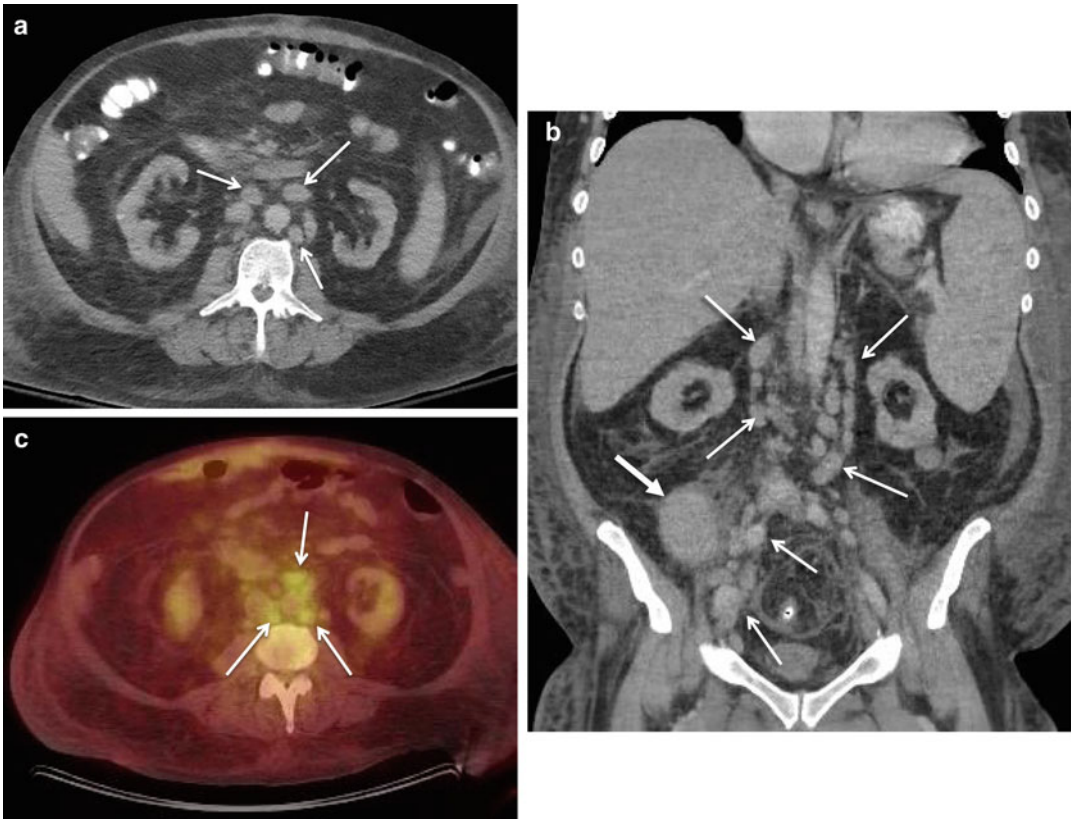


Fig. 30 CT of PTLD manifesting as lymphadenopathy. (a) Axial postcontrast CT image reveals multiple mildly enlarged retroperitoneal lymph nodes (*arrows*) in a patient with PTLD. (b) The corresponding coronally reformatted image shows the retroperitoneal lymphadenopathy, pelvic

lymphadenopathy (*arrows*), and a portion of the transplanted kidney in the right iliac fossa (*thick arrow*). (c) The PET/CT image shows hypermetabolic activity in the retroperitoneal lymph nodes (*arrows*)

and features much greater tissue contrast than CT. For example, posttransplant fluid collections are much more conspicuous through fat suppression and the extreme T2-hyperintensity of fluid compared with surrounding tissues and often better differentiated through MR imaging because of the unique T1 hyperintensity of the methemoglobin breakdown product in hemorrhage, the ability to visualize septation, and the higher conspicuity of the urinary excretion of contrast. Hematomas demonstrate hyperintensity on both T1- and T2-weighted images, whereas all other fluid collections are generally T1-hypointense and T2-hyperintense. Lymphoceles feature no specific MR findings, although occasional thin septa discriminate them from seromas and urinomas (Letourneau et al. 1987). Following intravenous

gadolinium administration, the accumulation of excreted contrast within the collection establishes the diagnosis of urinoma. Urinary obstruction is also better evaluated with MRI compared with CT. By acquiring MR urographic images using two techniques – extremely T2-weighted and delayed T1-weighted postcontrast images – the renal allograft collecting system, ureter, and point and etiology of obstruction are vividly portrayed (Fig. 32). However, renal calculi are less conspicuous on MR images compared with CT.

Regarding vascular complications, MR provides an alternative to CT in cases where iodinated contrast is contraindicated. MR angiography combines unenhanced and postcontrast techniques to evaluate the renal artery and vein, supplemented

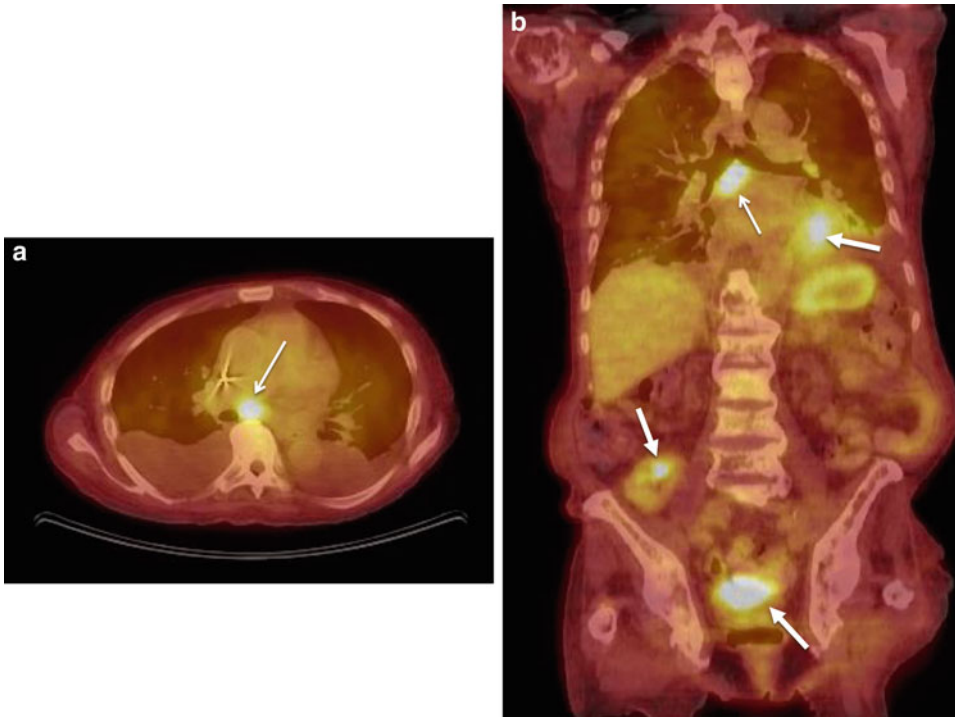


Fig. 31 PET/CT in PTLD. (a) The fused PET/CT axial image shows a hypermetabolic subcarinal lymph node (*arrow*) in a patient with PTLD following renal transplantation. (b) The corresponding coronal fused image shows

the subcarinal lymph node (*arrow*) with normal activity in the myocardium, renal collecting system and bladder (*thick arrows*)

by nonangiographic pulse sequences demonstrating parenchymal changes associated with vascular complications (such as segmental infarction, for example). The renal artery and vein are hyperintense on both unenhanced and enhanced MRA images with conspicuity maximized by fat suppression. The primary MR findings in renal artery stenosis and thrombosis are the same as seen on CT – (usually anastomotic) narrowing and absent enhancement or flow-related signal (in the case of unenhanced MRA), respectively. The iliac arteries are also included and reliably evaluated with MRA (Fig. 33). Associated renal infarcts are T2-hyperintense, nonenhancing, subcapsular, usually wedge-shaped foci, which help confirm the diagnosis of vascular insufficiency. The MR findings of renal venous stenosis and thrombosis also mirror the CT findings – (usually anastomotic) narrowing and lack of enhancement or flow-related signal, respectively. Additionally, in renal vein thrombosis, the renal allograft enlarges with

absent enhancement and relatively edematous T2-hyperintensity; subcapsular hemorrhage is also occasionally observed (Neimatallah et al. 1999).

MRI plays an ancillary role to CT and PET/CT regarding posttransplant malignancies, at least partly because of the greater challenge in covering the entire torso or body. Nonetheless, neoplastic tissue is generally more conspicuous on MRI compared with CT. Because of the relatively greater density of cells in malignant tumors, the diffusivity of water is restricted, reflected by hyperintensity on diffusion-weighted MR images with corresponding hypointensity on ADC map images. Diffusion restriction is especially prominent in lymphoma and PTLD. Additional MR features include T1-hypo- and T2-hyperintensity and mild homogeneous enhancement. Renal hilar involvement is notable for the lack of mass effect on vascular and collecting system structures disproportionate to size and central location.

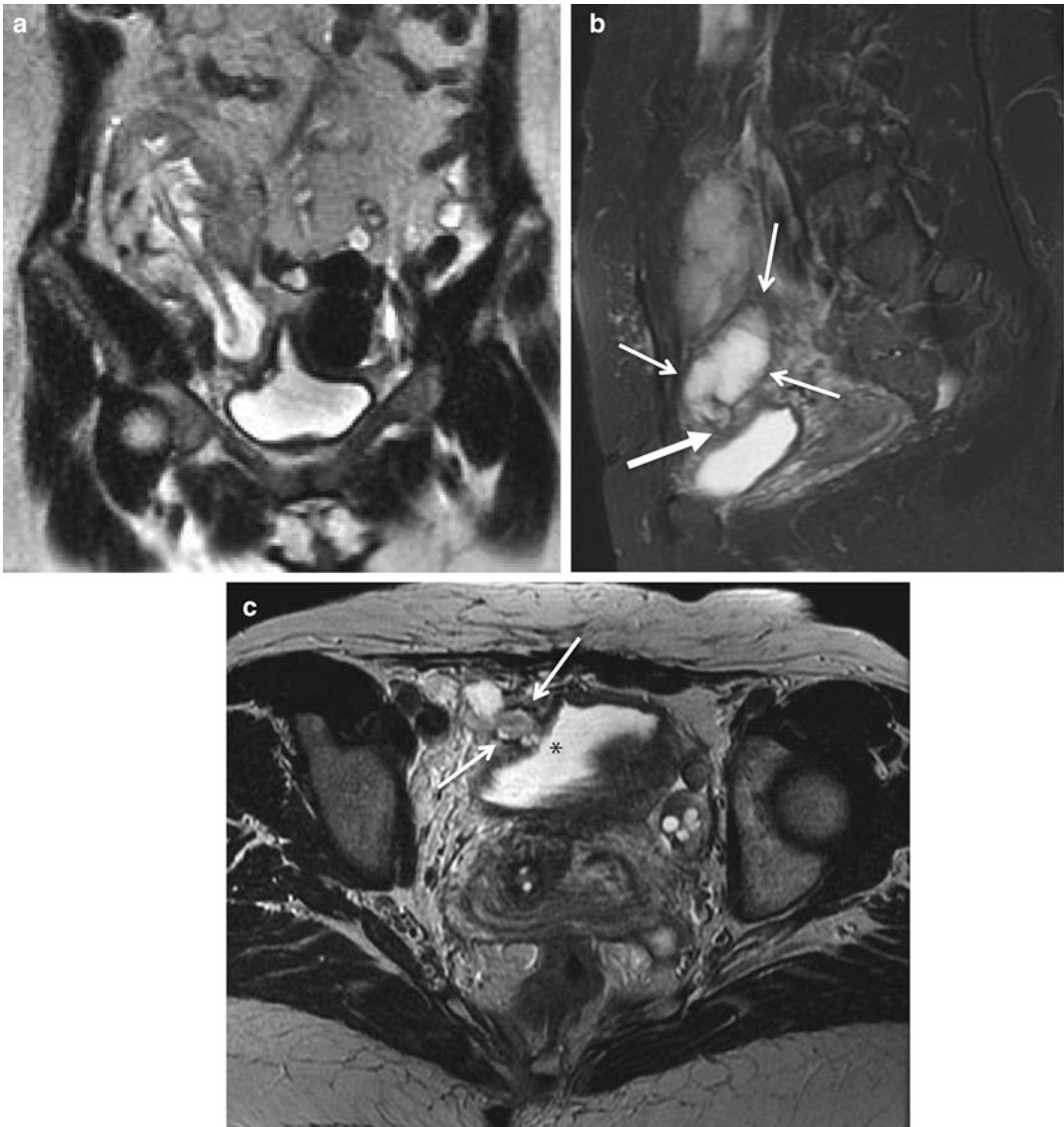


Fig. 32 MR urographic imaging demonstrating urinary obstruction. (a) Coronal T2-weighted image shows hydronephroureter involving the renal allograft in the right iliac fossa with a nephroureteral stent in place. (b) The sagittal T2-weighted, fat-suppressed image shows a

portion of the dilated ureter (arrows) proximal to a hypointense, fibrotic distal ureteral stricture (thick arrow). (c) Axial T2-weighted image shows the distal ureteral stricture (arrow) just proximal to the ureterovesical junction (asterisk, bladder)

Renal Scintigraphy

While ultrasound is the first-line modality to evaluate renal allograft failure, renal scintigraphy is a potentially useful alternative posing no threat to the allograft. Renal scintigraphy involves the intravenous administration of a radioisotope,

which emits gamma rays detected with a gamma camera, yielding images that illustrate the distribution of the radioactive agent. Regarding the radioisotope, technetium-labeled mercaptoacetyl-triglycine (Tc-99 m MAG3) is favored over technetium-labeled diethylenetriamine pentaacetic acid (Tc-99 m DTPA) because of its higher

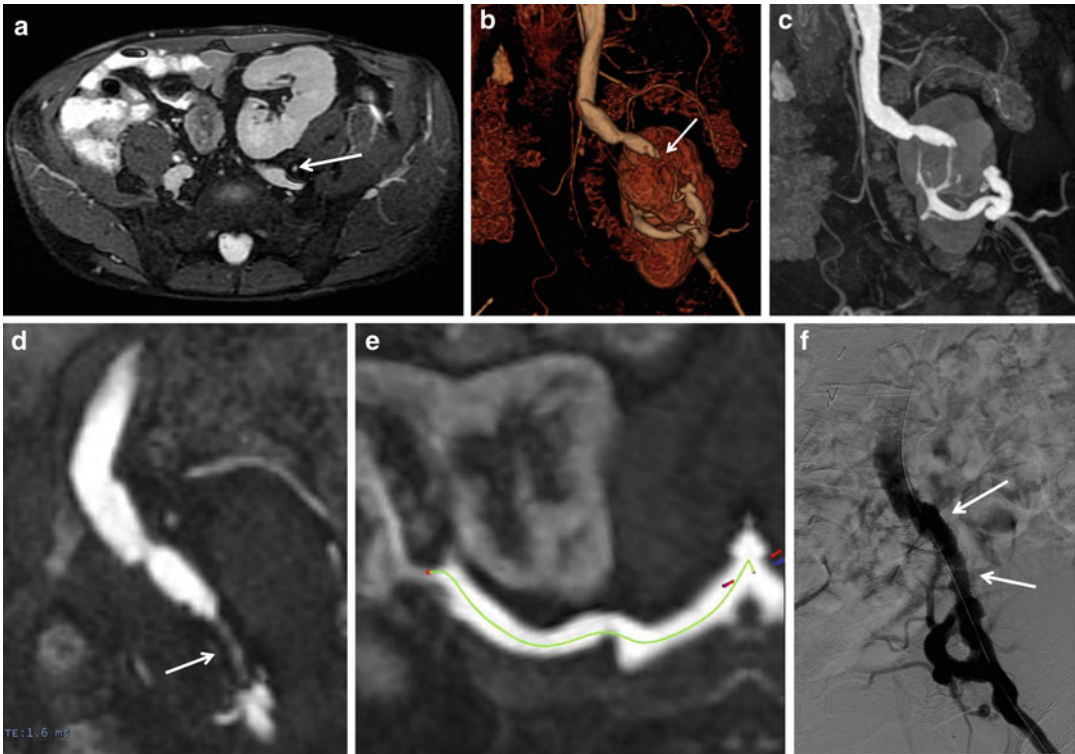


Fig. 33 MR findings in iliac artery stenosis. (a) Axial unenhanced MRA image shows virtual occlusion of the left external iliac artery (LEIA) with a minimal residual lumen (*arrow*). (b) The volume-rendered image from the contrast-enhanced MRA exaggerates the findings, giving the appearance of LEIA occlusion (*arrow*), but the renal artery appears relatively normal (*thick arrow*). (c) The maximal intensity projection image from the contrast-enhanced MRA mirrors the findings on the volume-

rendered image. (d) The obliquely coronally reformatted image from the contrast-enhanced MRA shows the critical LEIA stenosis (*arrow*) to better advantage. (e) The curved planar reformatted image of the renal artery from the contrast-enhanced MRA excludes high-grade stenosis. (f) Image from left iliac arteriography following LEIA stent placement (*arrows*) shows restoration of normal arterial caliber

extraction efficiency and greater utility in depressed renal function. Immediately following the injection of the radiopharmaceutical, serial images are acquired initially in 3 s frames for 1 min to assess arterial perfusion and then 15 s frames for approximately 30 min to evaluate radiotracer uptake and clearance. Planar images are obtained and semiquantitative analysis is performed by generating a time-activity curve of the renal allograft region-of-interest. The chief indications for renal transplant scintigraphy include:

Evaluation of renal perfusion (vascular occlusion)
 Evaluation of graft dysfunction (acute tubular necrosis, rejection, etc.)

Evaluation of peritransplant fluid collections
 Evaluation of urologic complications (leak and vesicoureteral reflux)

Renal artery thrombosis manifests scintigraphically as nonvisualization of the allograft. Renal artery stenosis results in diminished radiopharmaceutical uptake with normal parenchymal transit and without radiotracer retention. Acute tubular necrosis (ATN) classically demonstrates normal or near-normal perfusion with delayed radiopharmaceutical uptake and excretion and progressive cortical accumulation (Fig. 34) (Aktas 2014). However, in severe ATN, perfusion declines and the pattern overlaps with the appearance of rejection. Rejection typically exhibits

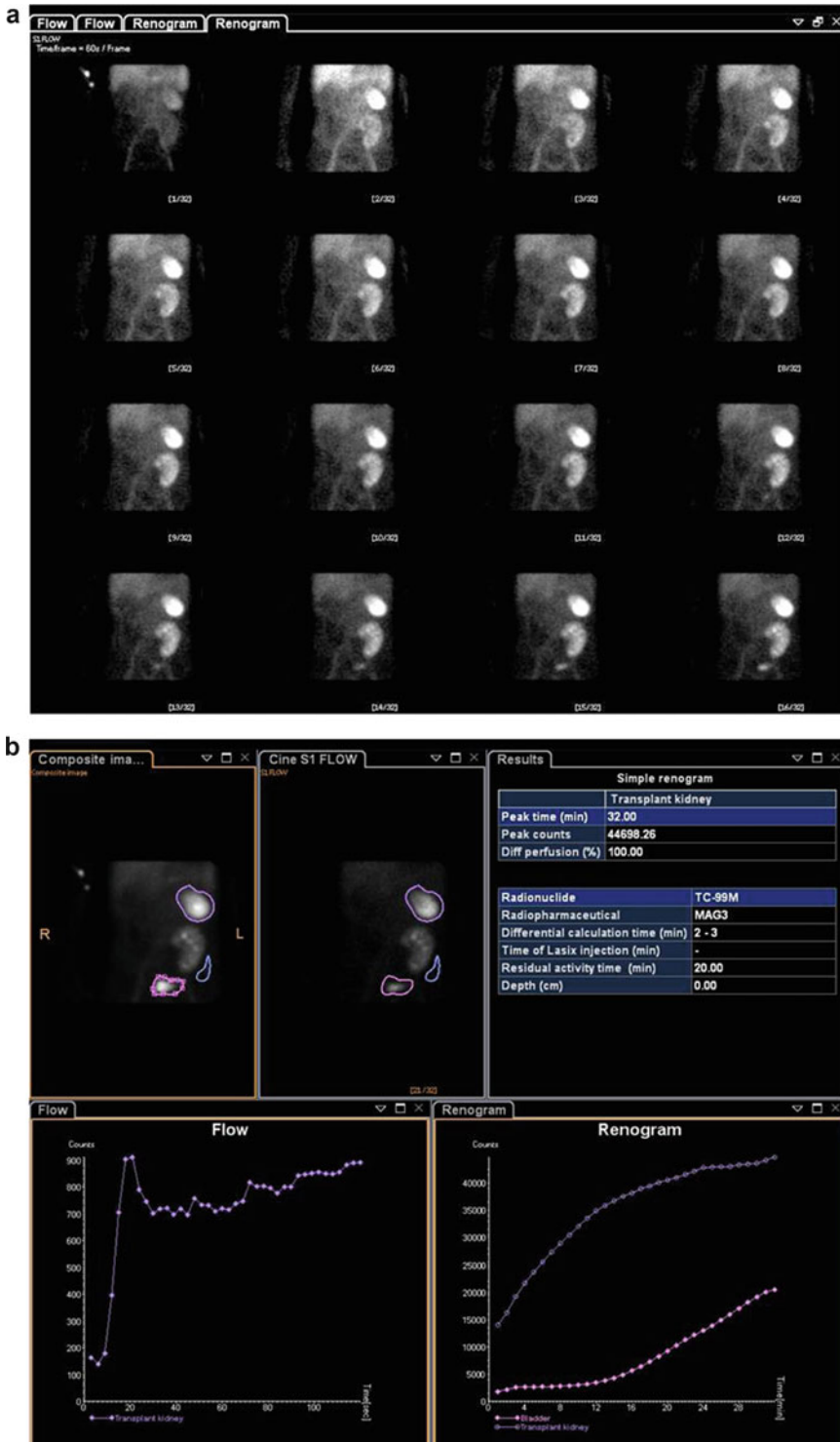


Fig. 34 Renal scintigraphy in acute tubular necrosis. (a) Serial images obtained during the renographic phase show progressive cortical radiotracer uptake without excretion.

(b) The time-activity curves (at the bottom) show normal flow (bottom left) and progressive cortical uptake (bottom right) of radiotracer

decreased perfusion, diminished uptake, and delayed excretion. Drug (cyclosporine) toxicity simulates rejection and potentially ATN scintigraphically with normal-to-depressed perfusion and parenchymal retention (Boubaker et al. 2006; Dubovsky et al. 1999). While considerable overlap in the scintigraphic appearances of etiologies of graft dysfunction limits definitive diagnosis, renal scintigraphy is useful to exclude other etiologies, such as urine leak or urinary obstruction (Sharfuddin 2011).

The scintigraphic evaluation of urinary obstruction is usually prompted by hydronephrosis detected sonographically. Renal scintigraphy adds diagnostic information by determining patency of the urinary tract in the setting of pelvic/lyceal

distention in terms of whether excreted radio-tracer reaches the bladder. Scintigraphy detects posttransplant fluid collections as a peritransplant photopenic area, which gradually accumulates excreted radiotracer only when the etiology is urinary leak forming a urinoma (Fig. 35).

Vescioureteral reflux (VUR) afflicts as many as 50–86% of patients following renal transplantation and is a consequence of ureteroneocystostomy (Ostrowski et al. 1999; Mastro Simone et al. 1993). The chief consequence of VUR is urinary tract infection and grading the degree of VUR with scintigraphy helps guide management, including open reimplantation or ureteroureterostomy to the native ureter when

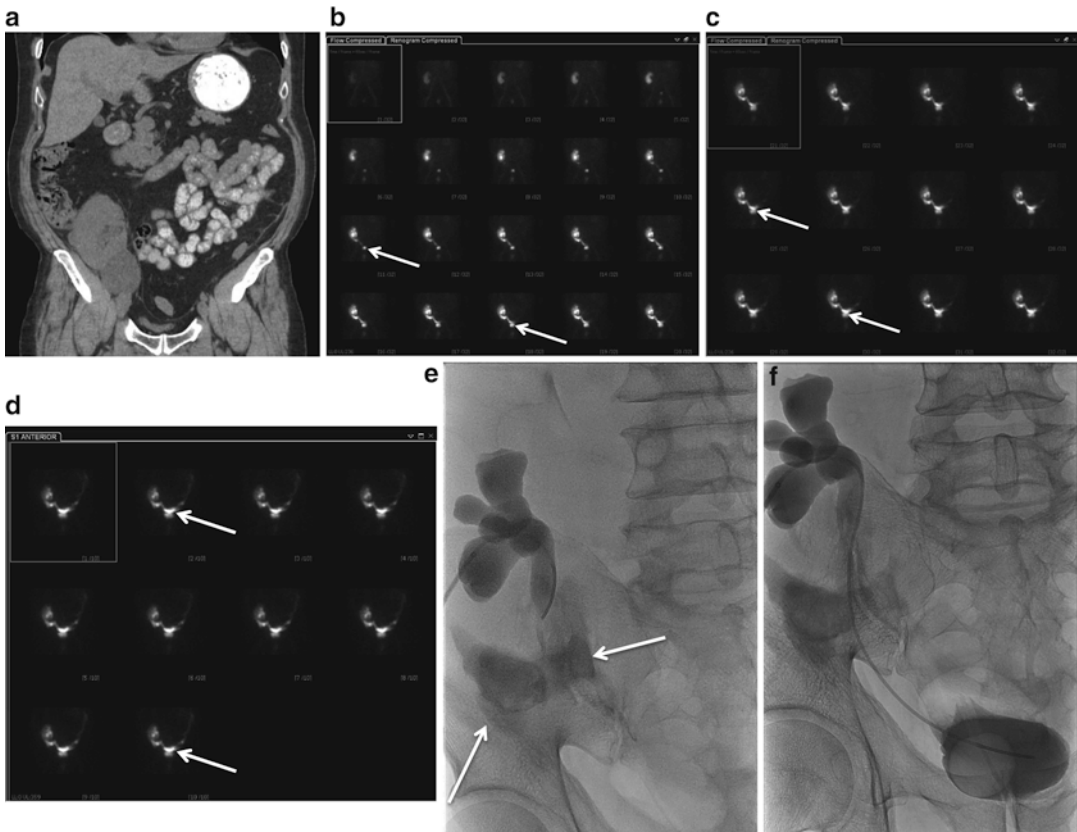


Fig. 35 Renal scintigraphy in urinary leak. (a) Coronally reformatted unenhanced CT image shows a fluid collection (*arrow*) abutting the lower pole of the allograft in the right iliac fossa. (b–d) Serial renographic images from renal scintigraphy reveals progressive accumulation of radiotracer outside the confines of the renal collecting system,

ureter, and bladder (*arrows*). (e) Image from a percutaneous nephrostomy shows extravasation of contrast (*arrows*) from the ureter. (f) Subsequent image shows placement of an antegrade nephroureteral catheter prior to stent placement

severe (Duty et al. 2013). VUR manifests scintigraphically with a “double peak” on the time-activity curve with the second peak reflecting refluxed radiotracer into the renal collecting system.

Interventional Radiology

With the rise of diagnostic imaging modalities, interventional procedures are generally reserved for the treatment of transplant complications. Image-guided procedures potentially address vascular and urinary complications and peritransplant fluid collections, as well as providing the means of obtaining histologic diagnosis when necessary for graft dysfunction. Renal allograft biopsy is usually undertaken under ultrasound guidance with real-time guidance optimizing targeting of glomeruli and preventing inadvertent injury to renal vascular structures. The complication rate varies from 0.06% to 13% (Ahmad 2004) with major complications leading to allograft failure exceedingly rare (Huraid et al. 1989; Bach et al. 1999).

Vascular disorders related to surgical technique and procedural complications amenable to interventional management include renal artery stenosis (RAS) and thrombosis and arteriovenous malformations and pseudoaneurysms. Although catheter-directed arteriography serves as the diagnostic gold standard for posttransplant RAS, the definition of hemodynamically significant transplant RAS has not been standardized. Stenoses starting at 50 up to 80% have been identified as significant (Lo et al. 1996; Krishnamoorthy et al. 2009). Transplant RAS usually presents to arteriography with refractory hypertension. With renal insufficiency, carbon dioxide may serve as an alternative contrast agent to iodinated contrast.

Arterial access is ideally achieved through the common femoral artery, although the brachial or axillary arteries serve as possible alternatives under certain circumstances. While most stenoses occur at the anastomosis, an inflow/preanastomotic stenosis potentially mimics transplant RAS clinically, which necessitates nonselective aorto-iliac arteriography (Fig. 33). Thereafter, anteroposterior and oblique projects of the iliac

arteries are obtained to localize the renal artery and identify and quantify the degree of stenosis (Fig. 36). At this point, percutaneous angioplasty and stenting can be performed. Postprocedural arteriography confirms resolution of the stenosis and stent location.

In the cases of (symptomatic) AVFs and (enlarging) pseudoaneurysms, transcatheter embolization is the treatment of choice. To minimize the loss of functioning allograft tissue, these lesions are approached with superselective embolization with metal coils (Kobayashi et al. 2007).

While graft thrombosis generally requires surgical thrombectomy, successful catheter-directed thrombolysis has been reported. However, it is contraindicated in the early postoperative period (within 2 weeks) because of the risk of sutural leakage at the immature anastomosis (Melamed et al. 2005; Rouviere et al. 2002).

Urologic complications amenable to IR management include ureteral obstruction and urinary leak. While noninvasive modalities generally secure the diagnosis of urinary obstruction, percutaneous nephrostomy provides a drainage pathway for recovery of renal function and a portal to subsequent percutaneous intervention. Additionally, the site and nature of the obstruction is demonstrated through antegrade nephrostography; the terminal ureter is often the culprit because of its vulnerability to ischemia as a consequence of its location far from the renal artery supplying the ureteral branch (Sandhu and Patel 2002). For high-grade perianastomotic strictures, balloon angioplasty post reasonably high success rates in the early posttransplantation period, ranging from 73% to 100% (Swierzewski et al. 1993; Bhagat et al. 1998; Bennett et al. 1986; Lojanapiwat et al. 1994; Fontaine et al. 1997). However, obstructions at other sites usually respond poorly to percutaneous treatment.

Urinary leaks usually occur at the distal ureter either related to ischemia or rejection or at the ureteroneocystostomy site. Once the diagnosis is established through either percutaneous aspiration of extravasated fluid or through scintigraphy, antegrade nephrostography accurately demonstrates the leakage site and percutaneous nephrostomy provides a diversionary pathway

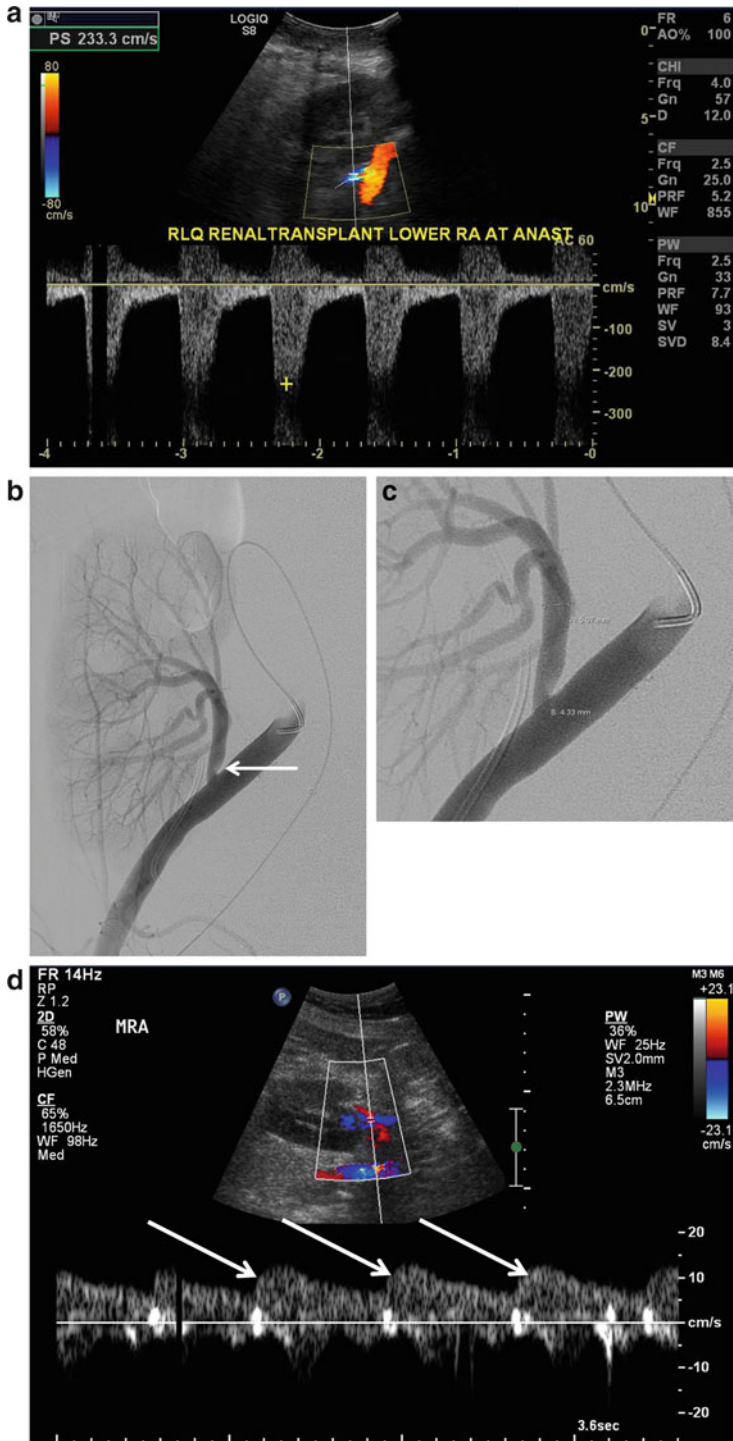


Fig. 36 (continued)

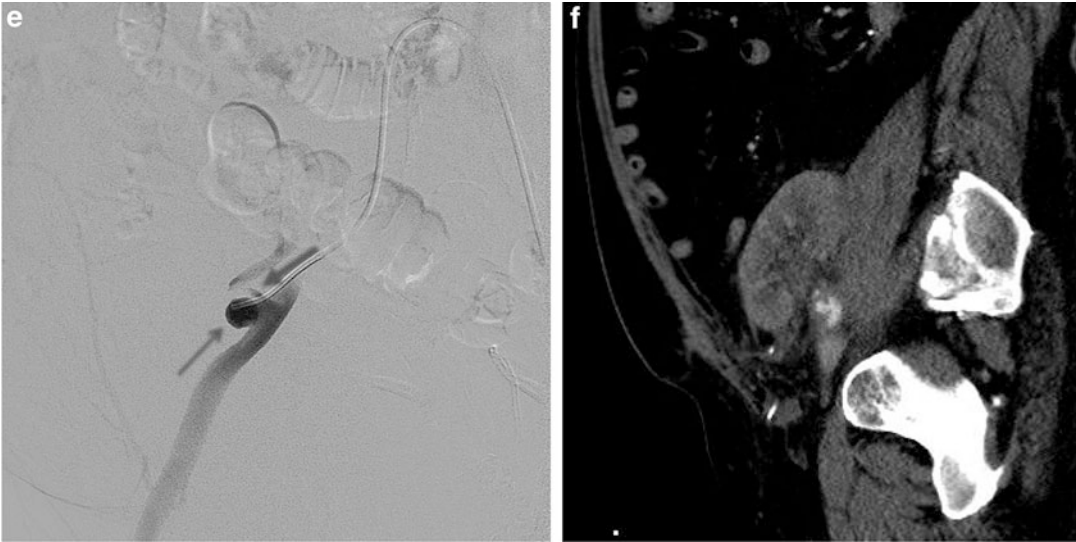


Fig. 36 Arteriography in renal transplant artery stenosis. (a) The spectral Doppler tracing of the proximal, post-anastomotic renal artery reveals elevated peak systolic velocity (233 cm/s), which is more than double the velocity in the external iliac artery (not shown). (b) Oblique projection from a catheter-directed arteriogram shows narrowing in the proximal renal artery (*arrow*). (c) Magnified view in the oblique projection with superimposed luminal diameter measurements shows the relatively mild degree of stenosis comparing the stenotic diameter

(4.33 mm) to the normal downstream diameter (5.07 mm). (d) Spectral Doppler tracing of the transplanted renal artery shows blunted waveform with a slow systolic upstroke (*arrows*). (e) Oblique projection from a right external iliac arteriogram reveals a pseudoaneurysm (*arrow*) at the anastomosis with an adjacent high-grade stenosis of the proximal renal artery (*thick arrow*). (f) Sagittal reformatted image from a CTA through the anastomosis shows the pseudoaneurysm (*arrow*)

for urinary flow, promoting ureteral healing (Fig. 35). Subsequent nephroureteral stent placement across the injured ureter with external nephrostomy drainage is a treatment option, although success rates vary widely and surgical revision is occasionally necessary.

Peritransplant fluid collections often require drainage for either diagnostic and/or treatment purposes. With graft dysfunction or symptoms arising from mass effect, percutaneous fluid collection aspiration is generally necessary. Seromas and hematomas undergo drainage only when large enough to exert mass effect and elicit symptoms or with superinfection (Fig. 37). Simple drainage of lymphoceles is associated with an 80–90% recurrence rate (Brockis et al. 1978) and indwelling catheter drainage combined with sclerotherapy posts a higher success rate (Johnson and Berry 2001). Urinomas are drained to alleviate mass effect and to preempt infection. Abscesses demand early percutaneous drainage.

Conclusion

Radiology factors into the preoperative planning and the postoperative management of renal transplantation. Choosing the most appropriate imaging modality requires an understanding of the properties and relative utility of each. Regarding donors in the preoperative planning setting, the primary objective of imaging is anatomic characterization and CT is the mainstay with its high spatial resolution to portray vascular anatomy and its ability to demonstrate parenchymal lesions, calculi, and collecting system anatomy. CTA imaging depicts small-caliber arteries, which affect the surgical approach, and delayed CT images demonstrate venous anatomy to help identify the more suitable donor venous drainage. The relatively high sensitivity for intrinsic vascular diseases, solid and cystic lesions, and collecting system anomalies and diseases also recommends

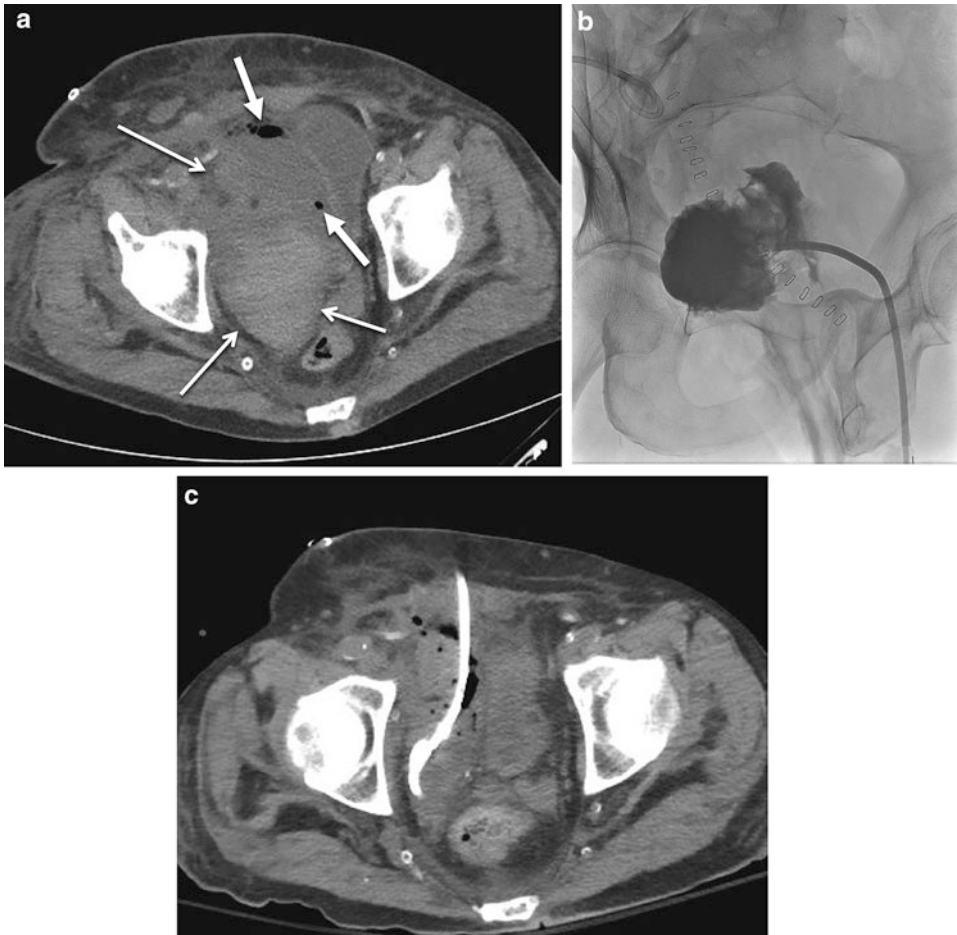


Fig. 37 Infected hematoma. **(a)** Axial unenhanced CT image shows a heterogeneous fluid collection (*arrows*) with layering dense material typical of a hematoma with punctate foci of gas (*thick arrows*) indicating infection displacing the bladder laterally (*asterisk*). **(b)** Fluoroscopic image obtained following ultrasound-guided drainage

catheter placement with contrast injection to confirm successful placement outlines the confines of the collection. **(c)** Axial unenhanced CT image following drainage catheter placement shows decreased size of the collection and mass effect on the adjacent bladder

CT and MRI generally serves as a reasonable alternative, with a limited sensitivity for nephrolithiasis.

Preoperative imaging of renal transplant recipients, aside from a chest X-ray and screening mammography, is generally limited to patients with peripheral and cardiovascular risk factors. In these patients, unenhanced CT versus CTA is used to assess the burden of atherosclerotic calcification and/or provide an overall assessment of the relevant arterial system, respectively. Cardiovascular disease screening is achieved with either nuclear scintigraphy or echocardiography

including either physical exercise or pharmacologic stress.

Routine posttransplant surveillance includes bone densitometry to assess the effects of long-term steroid administration. In the setting of graft dysfunction, imaging plays a major role and ultrasound is the most important imaging modality because of its noninvasiveness, availability, suitability of the relatively superficial renal allograft, and the ability to demonstrate anatomic and physiologic information. As such, US detects fluid collections, hydronephrosis and vascular complications, such as arterial occlusion or stenosis and

venous thrombosis, and guides most percutaneous treatments. Other complications, such as rejection and ATN, manifest with a nonspecific combination of parenchymal changes and elevation of the resistive index, prompting further workup to identify the etiology. CT plays an ancillary role in managing posttransplant complications, but provides greater anatomic coverage than US. While CTA provides confirmatory information regarding vascular complications, iodinated contrast is often avoided in the early posttransplant setting. However, CT is the first-line modality for PTLD, which generally manifests with either lymphadenopathy or allograft involvement in the form of a hilar mass or multifocal parenchymal lesions. PET/CT combines the sensitivity of hypermetabolism with the anatomic information provided by CT.

MRI also serves an ancillary role to assess posttransplant complications. Because of its exquisite tissue contrast, fluid collections are more accurately characterized compared with other imaging modalities. Obstructive uropathy is also vividly portrayed along with the etiology of obstruction, except in the case of calculi. Vascular complications are also well demonstrated with MRI, even without intravenous contrast, when contraindicated by renal insufficiency or contrast. Renal scintigraphy is a useful alternative to US in evaluating allograft dysfunction. By obtaining serial images for approximately 30 min after injecting a radioisotope (usually Tc-99 m MAG3), information regarding arterial perfusion and radiotracer uptake and clearance are obtained. This provides diagnostic information regarding possible vascular complications, graft dysfunction by generating time-activity curves, fluid collections (corresponding to photopenic regions), and urologic complications by demonstrating abnormal accumulation of radiotracer in a dilated collecting system in the case of obstructive uropathy or outside the collecting system in the case of extravasation.

Interventional radiology includes an array of procedures managing vascular and urologic complications and fluid collections. After confirmatory diagnostic arteriography, renal artery stenosis can be treated with angioplasty and stenting,

AVFs and pseudoaneurysms are treated with superselective transcatheter embolization. Urologic complications rely on percutaneous nephrostomy to establish an alternative urinary drainage pathway and access point for possible ureteral stent placement and for diagnostic antegrade nephrostography and potentially ureteral stricture angioplasty. Fluid collections requiring drainage are performed with imaging guidance – ultrasound is the modality of choice and CT provides an alternative in the setting of a poor acoustic window.

Radiology fulfills many roles in the life cycle of renal transplantation from donor screening, recipient anatomic assessment to diagnosing and treating posttransplant complications. Each modality has unique utility and understanding the respective properties and limitations of each is necessary to optimize patient care in the transplant setting.

Cross-References

- ▶ [Kidney Transplantation: Surgical Complications](#)
- ▶ [Living Donor Evaluation and Selection](#)
- ▶ [Medical Complications After Kidney Transplantation: Early](#)
- ▶ [Medical Complications After Kidney Transplantation: Late](#)

References

- Abrams HL (1983) Renal venography. In: Abrams HL (ed) *Abrams' angiography*, 2nd edn. Little, Brown, Boston, pp 1327–1364. ACR Committee on Drugs and Contrast Media. (2013)
- Absy M, Metreweli C, Matthews C, A.Al Khader A. (1987) Changes in transplanted kidney volume measured by ultrasound. *BJR* 60:525–529
- ACR Manual on Contrast Media, Version 9 (2013) Retrieved 13 Aug 2016 from: <http://www.acr.org/Quality-Safety/Resources/~media/37D844F1D4E1B9A3A2918DA9E28A3.pdf>
- Ahmad I (2004) Biopsy of the transplanted kidney. *Semin Interv Radiol* 21:275–281
- Aktas A (2014) Transplanted kidney function evaluation. *Semin Nucl Med* 44:129–145
- Ali A, Rajagopal P, Sayed A, Hakim N, David T, Papalois P (2012) Transplant of kidneys with small renal cell

- carcinoma in incompatible, heavily immunosuppressed recipients. *Ann R Coll Surg Engl* 94(6):e189–e190
- Andreoni KA, Weeks SM, Gerber DA et al (2002) Incidence of donor renal fibro-muscular dysplasia: does it justify routine angiography? *Transplantation* 73(7): 1112–1116
- Bach D, Wirth C, Schott G, Hollenbeck M, Grabensee B (1999) Percutaneous renal biopsy: 3 years of experience with the biopsy gun in 761 cases – a survey of results and complications. *Int Urol Nephrol* 31:15–22
- Bakker NA, Pruim J, de Graaf W, van Son WJ, van der Jagt EJ, van Imhoff GW (2006) PTLD visualization by FDG-PET: improved detection of extranodal localizations. *Am J Transplant* 6:1984–1985
- Bakker NA, van Imhoff GW, Verschuuren EA, van Son WJ (2007) Presentation and early detection of post-transplant lymphoproliferative disorder after solid organ transplantation. *Transpl Int* 20:207–218
- Balzer KM, Grottemeyer D, Pfeiffer T et al (2007) Fibromuscular dysplasia and renal transplantation. *Lancet* 369(9557):187
- Bennett LN, Voegeli DR, Crummy AB, McDermott JC, Jensen SR, Sollinger HW (1986) Urologic complications following renal transplantation: role of interventional radiologic procedures. *Radiology* 160:531–536
- Bhagat VJ, Gordon RL, Osorio RW et al (1998) Ureteral obstructions and leaks after renal transplantation: outcome of percutaneous antegrade ureteral stent placement in 44 patients. *Radiology* 209:159–167
- Bianchi E, Pascual M, Nicod M, Delaloye AB, Duchosal MA (2008) Clinical usefulness of FDG-PET/CT scan imaging in the management of posttransplant lymphoproliferative disease. *Transplantation* 85:707–712
- Bin PS, Kon KJ, Kyoung-Sik C (2007) Complications of renal transplantation: ultrasonographic evaluation. *J Ultras Med* 26(5):615–633
- Blondin D, Lanzman R, Schellhammer F, Oels M, Grottemeyer D, Baldus SE, Rump LC, Sandmann W, Voiculescu A (2010) Fibromuscular dysplasia in living renal donors: still a challenge to tomographic angiography. *Eur J Radiol* 75:67–71
- Borhani AA, Hosseinzadeh K, Almusa O, Furlan A, Nalesnik M (2009) Imaging of posttransplantation lymphoproliferative disorder after solid organ transplantation. *Radiographics* 29(4):981–1000
- Bosniak MA (1981) Angiomyolipoma (hamartoma) of the kidney: a preoperative diagnosis is possible in virtually every case. *Urol Radiol* 3:135
- Bosniak MA (1986) The current radiological approach to renal cysts. *Radiology* 158:1–10
- Boubaker A, Prior JO, Meuwly JY et al (2006) Radionuclide investigations of the urinary tract in the era of multimodality imaging. *J Nucl Med* 47:1819–1836
- Brockis JG, Hulbert JC, Patel AS et al (1978) The diagnosis and treatment of lymphocoeles associated with renal transplantation: a report of 6 cases and a review of the literature. *Br J Urol* 50:307–312
- Chai JW, Lee W, Yin YH et al (2008) CT angiography for living kidney donors: accuracy, cause of misinterpretation and prevalence of variation. *Korean J Radiol* 9(4):333–339
- Chowdhury AR, Chakraborty D, Bhattacharya P, Dey RK (2013) Multilocular cystic renal cell carcinoma: a diagnostic dilemma: case report in a 30-year-old woman. *Urol Ann* 5(2):119–121
- Curry NS, Cochran ST, Bissada NK (2000) Cystic renal masses: accurate Bosniak classification requires adequate renal CT. *AJR Am J Roentgenol* 175:339–342
- Cuttino JT, Clark RL (1990) The normal vasculature of the genitourinary tract: embryology, anatomy, and hemodynamics. In: Hillman BJ (ed) *Clinical urography*, vol 3. Saunders, Philadelphia, pp 2076–2091
- Davenport MS, Khalatbari S, Cohan RH, Dillman JR, Ellis JH (2013) Contrast material-induced nephrotoxicity and intravenous low-osmolality iodinated contrast material: risk stratification by using estimated glomerular filtration rate. *Radiology* 268(3):719–728
- Dubovsky EV, Russell CD, Bischo-Delaloye A et al (1999) Report of the radionuclides in nephrourology committee for evaluation of transplanted kidney (review of techniques). *Semin Nucl Med* 29:175–188
- Duty BD, Conlin MJ, Fuchs EF, Barry JM (2013) The current role of endourologic management of renal transplantation complications. *Adv Urol* 2013. Article ID 246520, 6 pages. <https://doi.org/10.1155/2013/246520>
- Edwards JM, Zaccardi MJ, Strandness DE Jr (1992) A preliminary study of the role of duplex scanning in defining the adequacy of treatment of patients with renal artery fibromuscular dysplasia. *J Vasc Surg* 15(4):604–611
- Einstein DM, Herts BR, Weaver R, Obuchowski N, Zepp R, Singer A (1995) Evaluation of renal masses detected by excretory urography: cost-effectiveness of sonography versus CT. *AJR* 164:371–375
- Eriksson P, Mohammed AA, De Geer J, Kihlberg J, Persson A, Granerus G, Nyström F, Smedby Ö (2010) Non-invasive investigations of potential renal artery stenosis in renal insufficiency. *Nephrol Dial Transplant* 25(11):3607–3614
- Ferguson RM, Henry ML (1993) *Transplantation and immunology*. JB Lippincott, Philadelphia, pp 516–524
- Fontaine AB, Nijjar A, Rangaraj R (1997) Update on the use of percutaneous nephrostomy/balloon dilation for the treatment of renal transplant leak/obstruction. *J Vasc Intervent Radiol* 8:649–653
- Fowler KAB, Locken JA, Duchesne JH, Williamson MR (2002) US for detecting renal calculi with nonenhanced CT as a reference standard. *Radiology* 222(1):109–113
- Frank I, Blute ML, Cheville JC, Lohse CM, Weaver AL, Zincke H (2003) Solid renal tumors: an analysis of pathological features related to tumor size. *J Urol* 170:2217–2220
- Freire M, Remer EM (2009) Clinical radiology features of cystic renal masses. *AJR* 192(5):1367–1372

- Grottemeyer D, Voiculescu A, Iskandar F et al (2009) Renal cysts in living donor kidney transplantation: long-term follow-up in 25 patients. *Transplant Proc* 41(10): 4047–4051
- Hariharan S (2006) Recommendations for outpatient monitoring of kidney transplant recipients. *Am J Kidney Dis* 47(4):S22–S36
- Harisingshani MG, Maher MM, Gervais DA, McGovern F, Hahn P, Jhaveri K, Varghese J, Mueller PR (2003) Incidence of malignancy in complex cystic renal masses (Bosniak category III): should imaging-guided biopsy precede surgery? *AJR* 180(3):755–758
- Harrison LH, Flye MW, Seigler HF (1978) Incidence of anatomical variants in renal vasculature in the presence of normal renal function. *Ann Surg* 188:83–89
- Ho VB, Choyke PL (2004) MR evaluation of solid renal masses. *Magn Reson Imaging Clin N Am* 12:413–427
- Hofmann LV, Smith PA, Kuszyk BS, Kraus E, Fishman EK (1999) Three-dimensional helical CT angiography in renal transplant recipients: a new problem-solving tool. *AJR* 173:1085–1089
- Huraib S, Goldberg H, Katz A et al (1989) Percutaneous needle biopsy of the transplanted kidney: technique and complications. *Am J Kidney Dis* 14:13–17
- Jinzaki M, Tanimoto A, Narimatsu Y et al (1997) Angiomyolipoma: imaging findings in lesions with minimal fat. *Radiology* 205:497–502
- Johnson SP, Berry RS (2001) Interventional radiological management of the complications of renal transplantation. *Semin Interv Radiol* 18:047–058
- Kahn PC (1973) Selective venography of the branches. In: Ferris EJ, Hipona FA, Kahn PC et al (eds) *Venography of the inferior vena cava and its branches*. Krieger, Huntington, pp 154–224
- Kanis JA (2016) Welcome to FRAX[®]. World Health Organization. Retrieved 26 April 2016 from: <https://www.shef.ac.uk/FRAX/>
- Kawamoto S, Montgomery RA, Lawler LP, Horton KM, Fishman EK (2003) Multidetector angiography for preoperative evaluation of living laparoscopic kidney donors. *Am J Roentgenol* 180:1633–1638
- Kawamoto S, Montgomery RA, Lawler LP, Horton KM, Fishman EK (2004) Multi-detector row CT evaluation of living renal donors prior to laparoscopic nephrectomy. *Radiographics* 24(2):453–466
- Kawamoto S, Fishman EK (2006) MDCT angiography of living laparoscopic renal donors. *Abdom Imaging* 31(3):361–373
- Kettritz U, Semelka RC, Siegelman ES, Shoent JP, Mitchell DG (1996) Multilocular cystic nephroma: MR imaging appearance with current techniques, including gadolinium enhancement. *J Magn Reson Imaging* 6:145–148
- Kobayashi K, Censullo ML, Rossman LL, Kyriakides PN, Kahan BD, Cohen AM (2007) Interventional radiologic Management of Renal Transplant Dysfunction: indications, limitations, and technical considerations. *Radiographics* 27(4):1109–1130
- Koga S, Tanabe K, Yagisawa TT et al (1996) Urologic complications in renal transplantation. *Transplant Proc* 28(3):1472–1473
- Koga S, Nishikido M, Inuzuka NS et al (2000) An evaluation of Bosniak's radiological classification of cystic renal masses. *BJU Int* 86:607–609
- Krishnamoorthy S, Gopalakrishnan G, Kekre NS, Chacko N, Keshava S, John G (2009) Detection and treatment of transplant renal artery stenosis. *Indian J Urol* 25(1):56–61
- Kyllönen L, Salmela K, Pukkala E (2000) Cancer incidence in a kidney-transplanted population. *Transpl Int* 13(S1):S394–S398
- Lee TG, Henderson SC, Freeny PC (1978) Ultrasound findings of renal angiomyolipoma. *J Clin Ultrasound* 6:150
- Letourneau JG, Day DL, Ascher NL, Castaneda-Zuniga WR (1987) Imaging renal transplants. *AJR* 150:833–838
- Linder R, Billing H, Tibell A et al (1989) Fibromuscular dysplasia in donor kidneys—experience with three cases. *Transpl Int* 2(4):228–231
- Lingard DA, Lawson TL (1979) Accuracy of ultrasound in predicting the nature of renal masses. *J Urol* 122(6):724–727
- Lipkin ME, Preminger GM (2013) Imaging techniques for stone disease and methods for reducing radiation exposure. *Urol Clin N Am* 40(1):47–57
- Lo CY, Cheng IK, Tso WK, Mak KO (1996) Percutaneous transluminal angioplasty for transplant renal artery stenosis. *Transplant Proc* 28:1468–1469
- Lojanapiwat B, Mital D, Fallon L et al (1994) Management of ureteral stenosis after renal transplantation. *J Am Coll Surg* 179:21–24
- Lopez-Ben R, Smith JK, Kew CE II, Kenney PJ, Julian BA, Robbin ML (2000) Focal post-transplantation lymphoproliferative disorder at the renal allograft hilum. *AJR Am J Roentgenol* 175:1417–1422
- Maki DD, Birnbaum BA, Chakraborty DP, Jacobs JE, Carvalho BM, Herman GT (1999) Renal cyst Pseudo-enhancement: beam-hardening effects on CT numbers. *Radiology* 213(2):468–472
- Martin G, Sundaram CP, Sharfuddin A, Govani M (2007) Asymptomatic urolithiasis in living donor transplant kidneys: initial results. *Urology* 70(1):2–5. discussion, 5–6
- Mastrosimone S, Pignata G, Maresca MC et al (1993) Clinical significance of vesicoureteral reflux after kidney transplantation. *Clin Nephrol* 40(1):38–45
- McCormack L, Hany TI, Hubner M et al (2006) How useful is PET/CT imaging in the management of post-transplant lymphoproliferative disease after liver transplantation? *Am J Transplant* 6:1731–1736
- Melamed ML, Kim HS, Jaar BG, Molmenti E, Atta MG, Samaniego MD (2005) Combined percutaneous mechanical and chemical thrombectomy for renal vein thrombosis in kidney transplant recipients. *Am J Transplant* 5:621–626

- Meyyappan RM, Rajaraman T, Senthil D (2012) Incidental solid renal mass in a cadaveric donor kidney. *Indian J Urol* 28(2):202–203
- Morcos SK (2014) Nephrogenic systemic fibrosis following the administration of extracellular gadolinium based contrast agents: is the stability of the contrast agent molecule an important factor in the pathogenesis of this condition? *Br J Radiol* 80:73–76
- Muglia VF, Teixeira SR, Romão EA, Cassini MF, de Andrade MF, Kato M, Nardin MEP, Tucci Jr S. (2013). Imaging in kidney transplantation. In: Rath T (ed) Current issues and future direction of kidney transplantation. InTech. <https://doi.org/10.5772/55074>
- Neimatallah MA, Dong Q, Schoenberg SO, Cho KJ, Prince MR (1999) Magnetic resonance imaging in renal transplantation. *J Magn Reson Imaging* 10:357–368
- Nikken JJ, Krestin GP (2007) MRI of the kidney – state of the art. *Eur Radiol* 17(11):2780–2793
- OPTN (2016) Guidelines for the medical evaluation of living kidney donors (Living Donor Committee). Retrieved 25 Aug 2016 from: https://optn.transplant.hrsa.gov/PublicComment/pubcommentPropSub_208.pdf
- Ostrowski M, Włodarczyk Z, Wesołowski T et al (1999) Influence of ureterovesical anastomosis technique on the incidence of vesicoureteral reflux in renal transplant recipients. *Ann Transplant* 4(1):54–58
- Pérez JA, Torres FG, Toribio AM, Fernández LK, Hayoun C, Naranjo ID (2013) Angio CT assessment of anatomical variants in renal vasculature: its importance in the living donor. *Insights Imaging* 4(2): 199–211
- Pfeiffer T, Böhner H, Voiculescu A et al (2002) Even severe renal artery fibromuscular dysplasia is no contraindication for living donor renal transplantation: report of two successful cases with venous grafting of the donor renal artery. *Transplant Proc* 34(8): 3113–3116
- Platt JF, Rubin JM, Ellis JH (1989) Distinction between obstructive and non-obstructive pyelocaliectasis: role of duplex Doppler ultrasound in evaluation. *AJR Am J Roentgenol* 153(5):997–1000
- Platt JF, Ellis JH, Rublin JM (1991) Renal transplant pyelocaliectasis: role of duplex Doppler ultrasound in evaluation. *Radiology* 179(2):425–428
- Pozniak MA, Balison DJ, Lee FT Jr, Tambeaux RH, Uehling DT, Moon TD (1998) CT angiography of potential renal transplant donors. *Radiographics* 18:565–587
- Prasad SR, Humphrey PA, Catena JR et al (2006) Common and uncommon histologic subtypes of renal cell carcinoma: imaging spectrum with pathologic correlation. *Radiographics* 26:1795–1806
- Raghavendra BN, Bosniak MA, Megibow AJ (1983) Small angiomyolipoma of the kidney: Sonographic-CT evaluation. *AJR* 141:575
- Rankin SC, Jan W, Koffman CG (2001) Noninvasive imaging of living related kidney donors: evaluation with CT angiography and gadolinium-enhanced MR angiography. *Am J Roentgenol* 177(2):349–355
- Regan F, Kuszyk B, Bohlman ME, Jackman S (2005) Acute ureteric calculus obstruction: unenhanced spiral CT versus HASTE MR urography and abdominal radiograph. *Br J Radiol* 78:506–511
- Remzi M, Ozsoy M, Klingler HC et al (2006) Are small renal tumors harmless? Analysis of histopathological features according to tumors 4 cm or less in diameter. *J Urol* 176:896–899
- Rendon RA, Stanietzky N, Panzarella T et al (2000) The natural history of small renal masses. *J Urol* 164: 1143–1147
- Rifkin MD, Needleman L, Pasto ME, Kurtz AB, Foy PM, McGlynn E, Canino C, Baltarowich OH, Pennell RG, Goldberg BB (1987) Evaluation of renal transplant rejection by duplex Doppler examination: value of the resistive index. *AJR Am J Roentgenol* 148:759–762
- Rouviere O, Berger P, Beziat C et al (2002) Acute thrombosis of renal transplant artery: graft salvage by means of intra-arterial fibrinolysis. *Transplantation* 73:403–409
- Sandhu C, Patel U (2002) Renal transplantation dysfunction: the role of interventional radiology. *Clin Radiol* 57:772–783
- Sant GR, Heaney JA, Ucci AA Jr, Sarno RC, Meares EM Jr (1984) Computed tomographic findings in renal angiomyolipoma: an histologic correlation. *Urology* 24:293–296
- Satyapal KS, Haffjee AA, Singh B, Ramsaroop L, Robbs JV, Kalideen JM (2001) Additional renal arteries: incidence and morphometry. *Surg Radiol Anat* 23(1): 33–38
- Saw KC, McAteer JA, Monga AG, Chua GT, Lingeman JE, Williams JC Jr (2000) Helical CT of urinary calculi. *Am J Roentgenol* 175(2):329–332
- Scheible W, Ellenbogen PH, Leopold GR (1978) Lipomatous tumors of the kidney and adrenal: apparent echographic specificity. *Radiology* 129:153
- Sebastià C, Quiroga S, Boyé R, Cantarell C, Fernandez-Planas M, Alvarez A (2001) Helical CT in renal transplantation: normal findings and early and late complications. *Radiographics* 21(5):1103–1117
- Sebastià C, Peri L, Salvador R, Buñesch L, Revuelta I, Alcaraz A, Nicolau C (2010) Multidetector CT of living renal donors: lessons learned from surgeons. *Radiographics* 30(7):1875–1890
- Sharfuddin A (2011) Imaging evaluation of kidney transplant recipients. *Semin Nephrol* 31:259–271
- Sharfuddin A (2014) Renal relevant radiology: imaging in kidney transplantation. *Clin J Am Soc Nephrol* 9(2):416–429
- Siegel CL, McFarland EG, Brink JA, Fisher AJ, Humphrey P, Heiken JP (1997) CT of cystic renal masses: analysis of diagnostic performance and interobserver variation. *AJR Am J Roentgenol* 169:813–818
- Silverman SG, Israel GM, Herts BR, Richie JP (2008) Management of the incidental renal mass. *Radiology* 249(1):16–31
- Singh AK, Sahani DV (2008) Imaging of the renal donor and transplant recipient. *Radiol Clin N Am* 46(1): 79–93

- Smith RC, Verga M, McCarthy S, Rosenfield AT (1996) Diagnosis of acute flank pain: value of unenhanced helical CT. *AJR Am J Roentgenol* 166:97–101
- Spring DB, Salvatierra O Jr, Palubinskas AJ et al (1979) Results and significance of angiography in potential kidney donors. *Radiology* 133(1):45–47
- Sudah M, Vanninen R, Partanen K et al (2001) MR urography in evaluation of acute flank pain: T2-weighted sequences and gadolinium-enhanced three-dimensional FLASH compared with urography. *AJR* 176(1):105–112
- Sun MRM, Ngo L, Genega EM et al (2009) Renal cell carcinoma: dynamic contrast-enhanced MR imaging for differentiation of tumor subtypes – correlation with pathologic findings. *Radiology* 253:793–802
- Swierzewski SJ 3rd, Konnak JW, Ellis JH (1993) Treatment of renal transplant ureteral complications by percutaneous techniques. *J Urol* 149:986–987
- Thomsen HS, Morcos SK, Almén T, Bellin MF, Bertolotto M, Bongartz G et al (2013) Nephrogenic systemic fibrosis and gadolinium-based contrast media: updated ESUR contrast medium safety committee guidelines. *Eur Radiol* 23(2):307–318
- Türkvatan A, Akinci S, Yildiz S, Olçer T, Cumhuri T (2009) MDCT for preoperative evaluation of vascular anatomy in living renal donors. *Surg Radiol Anat* 31(4):227–235
- Uflacker R (2006) Abdominal aorta and branches. In: Uflacker R (ed) *Atlas of vascular anatomy: an angiographic approach*, 2nd edn. Lippincott Williams & Wilkins, Philadelphia, pp 111–222
- Urban BA, Ratner LE, Fishman EK (2001) Three-dimensional volume-rendered CT angiography of the renal arteries and veins: normal anatomy, variants and clinical applications. *Radiographics* 21:373–386
- von Schulthess GK, Steinert HC, Hany TF (2006) Integrated PET/CT: current applications and future directions. *Radiology* 238:405–422
- Wang ZJ, Coakley FV, Fu Y, Joe BN, Prevrhal S, Landaras LA, Webb EM, Yeh BM (2008) Renal cyst pseudoenhancement at multidetector CT: what are the effects of number of detectors and peak tube voltage? *Radiology* 248(3):910–916
- Yang C-W, Shen S-H, Chang Y-H, Chung H-J, Wang J-H, ATL L, Chen K-K (2013) Are there useful CT features to differentiate renal cell carcinoma from lipid-poor renal Angiomyolipoma? *Am J Roentgenol* 201(5):1017–1028
- Yang L, Krefting I, Gorovets A, Marzella L, Kaiser J, Boucher R, Rieves D (2012) Nephrogenic systemic fibrosis and class labeling of gadolinium-based contrast agents by the Food and Drug Administration. *Radiology* 265(1):248–253
- Zagoria RJ (2000) Imaging of small renal masses: a medical success story. *AJR* 175:945–955
- Zhang S, Yuan J, Li W, Ye Q (2014) Organ transplantation from donors (cadaveric or living) with a history of malignancy: review of the literature. *Transplant Rev* 28:169–175